R. & M. No. 3765

R. & M. No. 3765

PROCUREMENT EXECUTIVE, MINISTRY OF DEFENCE

AERONAUTICAL RESEARCH COUNCIL
REPORTS AND MEMORANDA

A Technique for Analysing the Results of a Flutter Calculation

By J. C. A. BALDOCK

Structures Dept., R.A.E., Farnborough

LONDON: HER MAJESTY'S STATIONERY OFFICE

1975

PRICE £1·90 NET

A Technique for Analysing the Results of a Flutter Calculation

By J. C. A. BALDOCK
Structures Dept., R.A.E., Farnborough

Reports and Memoranda No. 3765*
October, 1973

Summary

A technique is presented for condensing a multi-degree-of-freedom flutter calculation so that similar flutter conditions are achieved with two degrees-of-freedom. Use is made of digital computer programmes, and the process is largely automatic.

Examples of the application of the technique are given, and show that systems can often be reduced to two normal modes, or to two orthogonal combinations of normal modes, and that these modes can be interpreted physically.

A detailed analysis of one of the derived two degree-of-freedom systems is made. This analysis uses a method restricted to a binary system, and so the condensation technique made possible the application of this method.

*Replaces R.A.E. Technical Report 73168—A.R.C. 35 211

LIST OF CONTENTS

1. Introduction

Flutter equations representing systems with many degrees-of-freedom can be readily solved with the aid of a digital computer. It is tempting to use a large number of degrees-of-freedom in order to avoid making excessive simplifications, or to cover any possible type of coupling, but there is then the danger of reaching a level of complexity at which it is difficult to identify the different types of flutter that may be revealed. This difficulty may hinder the use of previous experience of similar systems for the identification of important parameters. It is, of course, possible to vary data in a systematic manner to find important parameters, but the outcome of this approach can be a vast quantity of results for different combinations of varied data, and there is a risk of a general air of confusion caused by the sheer bulk of results to be assimilated.

If a given flutter condition can be represented with a two degree-of-freedom, or binary, system, the analysis of that condition is as simple as it can be, both because of the reduction to the minimum number of degrees-of-freedom and because specialised techniques are available[1] for the study of the binary. For the equivalent binary system to be of practical use, the two degrees-of-freedom should be of physical significance, or be capable of physical interpretation, to the flutter analyst. For this reason, purely mathematical techniques may not prove satisfactory. The technique described in this Report was, in fact, derived empirically with the physical significance of the equivalent binary system in mind.

The technique is applied using digital computer programmes with a small amount of analysis between the stages of the process. It does not necessarily yield a satisfactory result, but the failures have been few. The amount of additional computer time required is not large, compared with the time required for the basic solutions.

The technique is outlined in Section 2, and is illustrated and described in more detail by an example of its application. Section 3 contains a discussion of the technique, whilst Section 4 is devoted to an analysis of the equivalent binary systems derived from the example in Section 2. The analysis of Section 4 is given in detail in order to illustrate how the benefits of reducing a flutter problem to equivalent binary form can be fully realised. Thorough analysis of the equivalent binary is an essential sequel to the application of the technique for deriving the binary, and the potential of the graphical representation[1] of the binary in this context is well illustrated in Section 4.

2. The Technique

2.1. Introduction

The technique of condensing a multi-degree-of-freedom flutter problem into an equivalent binary may be conveniently divided into three stages. In the first stage, the problem is transformed so that the equations of motion are expressed in terms of normal modes of the system. In the second stage, a systematic examination of the normal mode equations is made, in which degrees-of-freedom are successively omitted and the resulting flutter characteristics are calculated. The object of this stage is to reduce the number of degrees-of-freedom, whilst retaining an acceptable approximation to the flutter characteristics of the original system. Where two of the normal modes are insufficient to achieve this object, a method of grouping degrees-of-freedom is used so that an equivalent binary system can be found in which each mode is a linear combination of two or more of the normal modes. The method of grouping ensures that the modes of the resulting equivalent binary have certain normal mode properties. The third stage consists of applying a matric transformation to the original equations of motion in order to obtain the equations of motion of the equivalent binary. The numerical values of the terms in the transforming matrices are determined from the second stage.

2.2. Basic Results of the Example

The technique is described by reference to results obtained from a flutter analysis of the rear fuselage, fin and rudders of an aircraft. This analysis was itself a part of a much more comprehensive analysis of the aircraft. The geometry of the system is shown in Fig. 1. The rear fuselage was assumed to be encastré in this example. From the structural analysis of the rear fuselage, fin and rudders, with the rudder jacks assumed to be rigid, the normal modes were found and the five lower frequency modes retained in this analysis. To these, were added two modes of upper and lower rudder rotation against rudder jacks of assumed equal stiffness KJ_0, J_0 being a standard stiffness and K a scaled stiffness. The aerodynamic forces in this example were found using two different sets of quasi-steady assumptions (referred to as Set 1 and Set 2). By the usual process of solving the equations for specific values of airspeed, flutter speeds and frequencies were found for different rudder jack stiffnesses K. These results are shown in Figs. 2 and 3, from which it may be seen that the different aerodynamic

assumptions give very different results, and, from the evidence of flutter frequencies shown, it appears that changing the aerodynamic data for the same stiffness K, can result in a different type of flutter becoming critical.

The frequencies of the modes in this representation, called the arbitrary modes, are given in Table 1.

2.3. Stage 1: Transformation to Normal Modes

It may be seen from Figs. 2 and 3 that interesting parts of the curves are given with values of $K^{\frac{1}{2}}$ of 0·324, 0·725 and 1·0. Taking these values in turn, with each set of aerodynamic assumptions, will lead to sets of flutter equations of motion with constant coefficients:

$$A\ddot{q} + (\sigma^{\frac{1}{2}}vB + D)\dot{q} + (v^2C + E)q = 0, \tag{1}$$

where q is a column matrix of generalised coordinates,
A is a matrix of structural inertia coefficients,
B is a matrix of aerodynamic damping coefficients,
D is a matrix of structural damping coefficients,
C is a matrix of aerodynamic stiffness coefficients,
E is a matrix of structural stiffness coefficients,
σ is atmospheric relative density and
v is scaled equivalent airspeed.

A typical physical deflection z is given by $z = Zq$, where Z is a matrix of deflection coefficients.

The first stage of the process is to transform equation (1) to normal coordinates. A computer programme takes the coefficients of the equations, finds the normal modes $\bar{q}$ from matrices A and E, and transforms and scales the original matrices so that new equations in the normal modes $\bar{q}$ are obtained.

For example, if the normal modes obtained are given by:

$$[q] = [T][\bar{q}], \tag{2}$$

where $[T]$ is a square matrix, and $[T]^{\mathrm{T}}$ is its transpose, then
$[\bar{A}] = [T]^{\mathrm{T}}[A][T]$, and $[\bar{A}]$ is made identical with the unit matrix
$[I]$ by an appropriate scaling procedure on $[T]$
$[B] = [T]^{\mathrm{T}}[B][T]$ etc.

The deflections in the normal modes are given by $[z] = [Z][T][\bar{q}]$.

With the new coefficients, exactly the same solutions to the equations of motion will be obtained as for the original coefficients, as long as all the normal modes are retained.

The frequencies of the modes in this normal mode representation for the example are given in Table 2.

2.4. Stage 2: Degree-of-Freedom Dropping

A computer programme takes the normal mode coefficients output by the programme described in 2.3, together with the flutter speed and frequency of the total system. It then deletes the elements of $\bar{q}$, one at a time, and tests whether the reduced set of equations has a critical flutter condition within a specified range* of the critical airspeed and frequency of the total set. If the reduced set of equations has a critical flutter condition within the specified range, a further element of $\bar{q}$ is deleted and the test applied again. If the reduced set of equations does not have a critical flutter condition within the specified range, the element of $\bar{q}$ just deleted is replaced and another element is deleted. The process continues until all the elements of $\bar{q}$, in a specified order, have been checked. The critical flutter speed and frequency given by the reduced $\bar{q}$, together with the associated amplitude and phase vectors, are recorded. Results for the example are shown in Tables 3 and 4.

It has been found that two normal modes are often sufficient to represent the flutter conditions of a larger problem, as Tables 3 and 4 show. Typical vectors, when more than two elements of $\bar{q}$ are necessary, are shown

* The range used in the example was ± 10 per cent on critical speed and ± 15 per cent on critical frequency. Some judgment is required in fixing these values. Those quoted would allow the elimination of, say, 5 modes, each resulting in a 2 per cent change in flutter speed. This would be considered acceptable. The result of each stage of the degree-of-freedom dropping is output by the programme. These are studied at the end of a run, and, if it is thought necessary, a run is repeated with modified tolerances, if, for example, the elimination of a single mode results in a 10 per cent change of flutter speed. Such a large change in one stage would be unwise, and smaller tolerances would be called for in this case.

in Figs. 4 and 5. It may be seen how, in most cases, the vectors tend to cluster around two directions. This feature has been observed in many examples. The plotting of the vectors when the minimum set of normal modes exceeds two is the only step in this process that is not the routine running of a standard computer programmes, and the clustering of the vectors in two directions is the only requirement for continuing the condensation process in a routine manner. Sometimes it is possible to achieve a good representation when the clustering is not obvious. Points h. and i. on Fig. 5 are examples of this. These points are considered further in Section 2.5.

2.5. Stage 3: Binary Transformation

The reduction to a binary system is effected by a transformation matrix $[t]$, of order $(n \times 2)$, where n is the order of the original matrices. $[t]$ is derived from the results of Stage 2, the degree-of-freedom dropping. This is described below, but there is an important feature of the form of $[t]$ which is conveniently described initially. The transformation effected by $[t]$ is, for instance:

$$[\bar{\bar{E}}] = [t]^{\mathrm{T}}[\bar{E}][t]$$

where $[\bar{E}]$ is output by stage 1,
and $[t]^{\mathrm{T}}$ is the transpose of $[t]$.

Stage 1 ouputs matrices of coefficients appropriate to normal modes, and so the structural inertia matrix $[\bar{A}](=[I])$ and the structural stiffness matrix $[\bar{E}]$ are diagonal. If, now, $[t]$ is formed so that any row of $[t]$ contains no more than one finite element, then it can easily be shown that the (2×2) matrices $[\bar{A}]$ and $[\bar{\bar{E}}]$ are diagonal. This property is found to have advantages which are discussed in Section 3.

With this in mind, the derivation of $[t]$ is based on the output of Stage 2 and depends on the form of this output.

(a) When Stage 2 has output a minimum $\bar{q}$, with only two elements, then, for example:

$$t = \begin{bmatrix} 0 & 0 \\ 1 & 0 \\ 0 & 1 \\ 0 & 0 \\ 0 & 0 \\ 0 & 0 \\ 0 & 0 \end{bmatrix} \quad \text{with } n = 7$$

where, in this case, the equivalent binary consists of modes 2 and 3 of the original 7.

There is an arbitrary value of unity in the elements marking the two specified elements of the original $\bar{q}$, and the effect of this transformation is to select the (2×2) matrices appropriate to the two required degrees-of-freedom.

(b) When Stage 2 has output a minimum $\bar{q}$ with more than two elements, then $[t]$ is formed by reference to the plot of the critical vectors.

Each column of $[t]$ is allocated to one of the two directions that are usually indicated by the clustering of the vectors, and the elements in each column are proportional to the amplitudes of the vectors allocated to that direction.

For example,

$$[t] = \begin{bmatrix} 1 & 0 \\ \alpha & 0 \\ 0 & 1 \\ -\beta & 0 \\ 0 & \gamma \\ 0 & 0 \\ 0 & 0 \end{bmatrix} \quad \text{with } n = 7$$

where $1, \alpha, -\beta$ are the relative vector amplitudes in one direction, and $1, \gamma$, are the relative vector amplitudes in the other direction.

Figs. 4 and 5 give examples of the form of $[t]$ for typical Stage 2 outputs. It should be noted that no attempt is made to include the components of the vectors in one specific direction. This reflects the empirical nature of this stage. Obviously, if the vectors to be associated lay in precisely the same direction, the elements in $[t]$ would accurately represent this. If the vectors are nearly in the same direction, factors proportional to the cosines of small angles could be introduced but, in view of the fact that this stage is essentially an approximation, this has not usually been done. A similar point arises when the clustering of the vectors into two directions is not obvious. Examples of this are points h. and i. on Fig. 5, for which there is some doubt about whether normal mode 3 should be associated with mode 2 or with mode 4. The obvious compromise, to resolve mode 3 in the directions of the other modes, would result in finite elements in row 3 of each of the columns of $[t]$, which is undesirable as it results in non-diagonal matrices $[\bar{\bar{A}}]$ and $[\bar{\bar{E}}]$. Instead, both possibilities for mode 3 were developed; the full amplitude was associated separately with modes 2 and 4. The $[t]$ matrices shown on Fig. 5 resulted in the representation shown in Fig. 3. The alternatives did not give such good agreement with the full system.

The binary transformation is carried out by a computer programme which uses the normal mode coefficients output from Stage 1 and the matrices $[t]$.

For example, with $[\bar{q}] = [t][q]$,

$$[\bar{\bar{E}}] = [t]^{\mathrm{T}}[\bar{E}][t] \qquad [\bar{\bar{E}}] \text{ is of order } (2 \times 2)$$

etc., and

$$[z] = [Z][T][t][\bar{q}].$$

2.6. Stage 4: Checking the Binary System

The binary transformation programme of 2.5 will produce sets of binary coefficients. The equations associated with these coefficients are solved in the same way as for the basic results for the original system. The results from the original system and from the binary are then compared for the following features:

(a) critical flutter speed,

(b) critical flutter frequency and

(c) variation with airspeed of the frequency and decay of the critical root.

Only if there is reasonable agreement in all of these features, may it be concluded that the binary system represents the original system.

The agreement achieved with some of the points in the example given here is shown in Tables 3 and 4.

The flutter speeds from binary solutions are superimposed on those from the complete system on Figs. 2 and 3. The binary solutions are marked with a letter.

For jack stiffness $K^{\frac{1}{2}} = 0{\cdot}324$ and Set 1 aerodynamics, the variation of mode frequencies and dampings with airspeed is shown, in Fig. 6, for the original system, and, in Figs. 7 and 8 for the binary equivalents.

For jack stiffness $K^{\frac{1}{2}} = 0{\cdot}725$ and Set 2 aerodynamics, the variation of mode frequencies and dampings with airspeed is shown, in Fig. 9, for the original system, and, in Figs. 10 and 11, for the binary equivalents.

It may be seen that there is good agreement, and there can be little doubt that the equivalent binary systems contain the essence of the flutter conditions of the original system.

The mode shapes associated with the binary systems are also found. Some of these are described in Section 4, together with an example of the analysis that is possible with the binary equivalent systems.

3. Discussion of the Binary Condensation Technique

There are probably many binary transformations that will result in a binary system with similar flutter speed and frequency to the original system. For instance, if the critical vector of any system is found at flutter, a binary transformation matrix t, with (real) columns proportional to the real and imaginary parts of the vector will result in a binary system with the same flutter speed. However, Section 1 states that the two degrees-of-freedom should be of physical significance, and this is unlikely to be the case with this transformation.

Normal modes have physical significance at zero airspeed, and the graphical representation technique[1], useful in the analysis of the equivalent binary, requires the binary to be in normal modes. These considerations suggested that the use of normal modes would be fruitful. The first transformation is to normal coordinates (Stage 1), and it may be seen from Tables 3 and 4 that degree-of-freedom dropping (Stage 2) often results directly in showing that two normal modes represent the flutter condition adequately. In cases when more than two normal modes remain, the form of the binary transformation matrix $[t]$ (Stage 3) was chosen so that, when the

transformation is applied to normal mode coefficients, a diagonal binary inertia matrix $[\bar{A}]$ and structural stiffness matrix $[\bar{\bar{E}}]$ results. This follows from the form adopted for $[t]$—in each row, if one element is finite, the other element is zero, as pointed out in Section 2.5. The binary degrees-of-freedom, therefore, have one of the properties of normal modes, although they are not orthogonal through the matrices $[\bar{A}]$ and $[\bar{\bar{E}}]$ with *all* of the true normal modes. Stages 1 and 3 of the technique as described, result in the simplest evolution of two modes, which form an equivalent binary system and which are orthogonal through the structural inertia and stiffness matrices. This simplicity makes it more likely that the physical significance of the normal modes will be retained in the equivalent binary modes.

Other approaches tend to lead to more complication. For instance, it has been found that if the normal mode transformation (Stage 1) is omitted, this often results in less distinct clustering in the vector output after degree-of-freedom dropping (Stage 2). Stage 3, the choice of the binary transformation, would, then, not be so obvious, and the form of $[t]$ that leads to diagonal $[\bar{A}]$ and $[\bar{\bar{E}}]$ would probably have to be abandoned. In this case, another stage would be necessary before Ref. 1 could be applied, since this requires diagonal $[\bar{A}]$ and $[\bar{\bar{E}}]$. The likelihood of any physical significance in the equivalent binary modes would be reduced by this last stage.

The standard method of Section 2 has worked well with the example quoted here and in other examples, and has, in particular, resulted in mode shapes with physical significance. Some of these are described in Section 4.

4. Analysis of the Binary Systems

4.1. Introduction

Figs. 2 and 3 show the degree of representation achieved with the derived binary systems. A description of the binary condensation process is the main purpose of this Report. However, some of the mode shapes associated with the binary degrees-of-freedom will be described, and one example of the type of analysis made possible when the system has been reduced to a binary will be presented.

In Section 4.2, modes will be discussed in relation to the general form of Figs. 2 and 3.

In Section 4.3, the Graphical Representation[1] will be briefly described and its application to a particular point given in Section 4.4.

4.2. The General Form of Figs. 2 and 3

It is explained in Section 2.5 that Stage 3, the binary transformation, gives, as well as the binary flutter coefficients, the physical deflections in the two degrees-of-freedom, that is the shapes of the modes involved in the flutter. As well as these modal shapes, there will also be available the shapes of the original modes, and of the normal modes from Stage 1. It should, therefore, always be possible to judge whether the Stage 3 binary modes are capable of physical interpretation by comparing them with the full system modes. For instance, in the example used here the binary modes were often different from the full system modes by the elimination of the rotation of one of the rudders. In general, the normal modes showed rotation of both rudders, due to inertia couplings, but the overall result of degree-of-freedom dropping and Stage 3 was often the removal of, or reduction in, the rotation of one of the rudders if this rotation was not significant in the flutter being considered.

The modes found for all the binary points are not presented here, but it is hoped enough examples are given to explain their usefulness.

Study of the mode shapes associated with points a, b and c on Fig. 2, with Set 1 aerodynamics, indicates that the branch of flutter represented by these points is due predominantly to coupling between the rear fuselage and fin fundamental mode and a mode containing upper rudder rotation together with some fin twist which increases as the jack stiffness K increases. As an example, Figs. 12 and 13 show the two modes associated with point c. This point is for a high value of the jack stiffness, and Fig. 13 shows that the second mode has appreciable fin twist, and that this feature results in the nodal line over the upper part of the fin being forward of the hinge line. The importance of this is shown in Section 4.4.

Study of the modes associated with the binary systems, with Set 2 aerodynamics on Fig. 3, shows that a similar type of flutter is given by the curves containing points f. and k. Therefore, for this type of flutter, both aerodynamic assumptions give similar flutter speeds at low values of jack stiffness K (compare a. on Fig. 2 with f. on Fig. 3), whereas Set 2 aerodynamics results in much higher flutter speeds at higher values of K (compare c. on Fig. 2 with k. on Fig. 3). At intermediate jack stiffnesses, Set 2 aerodynamics does not lead to a critical flutter coupling of this type.

The detailed reasons for the differences between points c. and k. are indicated in Section 4.4.

On Fig. 2, with Set 1 aerodynamics, study of the mode shapes indicated that the branch represented by points d. and e. is due predominantly to coupling between the rear fuselage and fin first overtone mode and the lower

rudder rotation mode. The equivalent branch, with Set 2 aerodynamics, on Fig. 3 is that represented by points g., h. and i. As an example the modes associated with point i. are shown in Figs. 14 and 15. It may be seen from Figs. 2 and 3 that there are considerable differences between the results obtained using Set 1 and Set 2 aerodynamics for this type of flutter. With Set 1 aerodynamics at low values of jack stiffness K, the flutter speed is higher than with Set 2 aerodynamics. As K is increased, with Set 1 aerodynamics the flutter speed increases until a limiting value of K is reached, beyond which this type of flutter is eliminated. With Set 2 aerodynamics, on the other hand, there is little variation of flutter speed with K.

On Fig. 3, with Set 2 aerodynamics, study of the mode shapes indicated that the branch represented by points j. and l. is due to coupling between the fin twist mode and the upper rudder rotation mode. This type of flutter does not appear on Fig. 2, with Set 1 aerodynamics, up to the maximum speed investigated.

4.3. The Graphical Representation[1] of a Flutter Condition

In the Graphical Representation, the equations of motion are recast so that the zero value of the Routh Test Function T_3 (i.e. the critical flutter condition) is obtained at the intersection of a conic and a straight line. The coordinates chosen are ω^2, proportional to the square of frequency, and y, proportional to the square of equivalent airspeed. The problem is scaled so that the inertia matrix $[\bar{\bar{A}}]$ is the unit matrix.

In Fig. 16, for example, the conic for the atmospheric relative density, σ, equal to zero, depends on the aerodynamic stiffness coefficients $[\bar{\bar{C}}]$ and the structural stiffness coefficients $[\bar{\bar{E}}]$. The conic with σ equal to unity differs from that with σ equal to zero due to a comparatively simple expression involving aerodynamic damping coefficients $[\bar{\bar{B}}]$. The straight line depends on aerodynamic damping coefficients $[\bar{\bar{B}}]$, aerodynamic stiffness coefficients $[\bar{\bar{C}}]$ and structural stiffness coefficients $[\bar{\bar{E}}]$. For convenience, the straight line is called the 'damping' line, because it is more dependent on $[\bar{\bar{B}}]$ than is the conic. Properties of the conic and the damping line (for example, the values of the conic and the damping line at speed parameter y equal to zero, the values of y for limiting values of the conic, the slope of damping line) are given in Ref. 1 as expressions containing the flutter coefficients. The expressions enable visual analysis of the conic and damping line to be interpreted in terms of the binary flutter coefficients.

4.4. Effect of Aerodynamic Assumptions on Point c., Fig. 2

Point c. on Fig. 2 arises from the coupling between the rear fuselage/fin fundamental mode and the upper rudder rotation mode. With Set 1 aerodynamics the scaled critical flutter speed is 1·35, while, with the same binary system, but Set 2 aerodynamics, the scaled critical flutter speed was computed to be 1·88. The reasons for this difference are investigated using the mode shapes for the binary degrees-of-freedom in Figs. 12 and 13, together with the binary coefficients and the Graphical Representation[1] of the binary with Set 1 and Set 2 aerodynamics shown in Figs. 16 and 17.

From Figs. 16 and 17, it may be seen that the lower flutter speed with Set 1 aerodynamics is attributable to the following features of the diagrams:

(a) Set 1 aerodynamics results in a lower value of the limiting y for the conic with atmospheric relative density σ equal to zero, and this feature appears to be due to differences in the slope of the conic for the higher frequency point at y equal to zero,

(b) the effect of atmospheric relative density σ on the conic is smaller with Set 1 aerodynamics.

In Ref 1 expressions in terms of flutter coefficients for these features are listed. They are discussed in Appendix A with the binary flutter coefficients for Set 1 and Set 2 aerodynamics, and it is shown that the most significant differences in coefficients are those between c_{21} and c_{22}. Since quasi-steady strip theory is being used here, each aerodynamic coefficient can be expressed in terms of contributions from the aerodynamic derivatives, which are defined in Appendix B and listed in Table 5. It is a simple matter, using the transformation programmes of Stages 1 and 3 to find these derivative contributions, and, in Table 6, the contributions to c_{21} and c_{22} with Set 1 and Set 2 aerodynamics are compared. It can be seen from Table 6 that the differences between the coefficients are mostly due to differences between values of $(-m_\alpha)$ and $(-m_{\beta u})$.

Appendix B.2 shows that the position of the local centre-of-lift is given by the ratio $(-m_\alpha)/(l_\alpha)$ or $(-m_{\beta u})/(l_{\beta u})$. Since l_x and $l_{\beta u}$ are similar, it follows that the differences in $(-m_\alpha)$ and $(-m_{\beta u})$ describe differences in local centres-of-lift.

From the values of the derivatives in Table 5, the positions of the local centre-of-lift are:

(a) with Set 1 aerodynamics,

due to incidence α, 0·25c aft of leading edge

due to upper rudder rotation βu, 0·50c aft of leading edge

(b) with Set 2 aerodynamics

due to incidence α, 0·30c aft of leading edge

due to upper rudder rotation βu, 0·67c aft of leading edge.

The significance of these differences may be seen by considering the derivation of aerodynamic stiffness coefficient c_{rs}. This coefficient is derived from the work done by the aerodynamic forces due to mode s in a small displacement in mode r. For both c_{21} and c_{22}, the major contributions are seen, from Table 6, to be from the lift due to incidence (l_α and $(-m_\alpha)$) and the lift due to upper rudder rotation ($l_{\beta u}$ and $(-m_{\beta u})$). Therefore, the essential differences between Set 1 and Set 2 aerodynamics for c_{21} and c_{22} arise from the differences in the work done by the two sources of lift in a small displacement in mode 2 (Fig. 13), and these can be deduced by considering the two centres-of-lift and the deflections in the mode. To assist in this, the centres-of-lift quoted above are superimposed on the mode 2 shape in Fig. 13. It may be seen how, over the upper part of the fin, the nodal line is close to the different centres-of-lift. This is due to the fin incidence in the mode, and it results in there being large differences in deflection at the different centres-of-lift. This is responsible for the differences in c_{21} and c_{22}. Thus there are two sources for the differences:

(a) the differences in the centres-of-lift—an aerodynamic effect,

(b) the fin incidence in the mode, which results in the nodal line being forward of the rudder hinge, and, therefore, at chordwise stations close to the centres-of-lift—a structural effect.

The analysis has, therefore, revealed the importance of a combination of aerodynamic and structural features, and the accuracy of the flutter estimates can now be assessed by concentrating on the accuracy of the data for each feature.

The conclusions could, no doubt, have been reached by other methods, by, for instance, variations of individual aerodynamic derivatives in the complete calculation. This would have certainly involved a great deal more computation. It would also have been more complicated, as Fig. 2 shows that three types of flutter, all possibly varying in a different way with derivatives, would have had to be identified, and the pin-pointing of a particular aerodynamic effect on a particular mode shape would have required the additional solution of cases with reduced degrees-of-freedom. At all stages this alternative approach would have been tentative. On the other hand, the technique described above in Section 2 works progressively towards a positive result.

5. Concluding Remarks

The example of the technique that has been described has shown that it is possible to condense the flutter conditions in a multi-degree-of-freedom flutter analysis to equivalent two degree-of-freedom systems, in which the associated modes have physical significance. The technique uses digital computer programmes, is largely automatic, and the additional computer time required is not large.

One advantage of being able to study a two degree-of-freedom system has been shown by the use, with an example, of the Graphical Representation[1] of the binary. In this example, significant aerodynamic and structural features have been revealed.

Acknowledgments

The author gratefully acknowledges the value of discussion with Mr. H. P. Y. Hitch and Mr. B. W. Payne of the British Aircraft Corporation, and with Mr. Ll. T. Niblett and Mr. R. J. Davies of Structures Department, R.A.E., who also wrote the computer programmes used in this work.

LIST OF SYMBOLS

$A, \bar{A}, \bar{\bar{A}}$	Matrices of structural inertia coefficients
$B, \bar{B}, \bar{\bar{B}}$	Matrices of aerodynamic damping coefficients
$D, \bar{D}, \bar{\bar{D}}$	Matrices of structural damping coefficients
$C, \bar{C}, \bar{\bar{C}}$	Matrices of aerodynamic stiffness coefficients
C_{rs}	Typical element of C
$E, \bar{E}, \bar{\bar{E}}$	Matrices of structural stiffness coefficients
J_0	Standard rudder jack stiffness
K	Scaled rudder jack stiffness
$n_{\frac{1}{2}}$	Cycles to half amplitude
$q, \bar{q}, \bar{\bar{q}}$	Column matrices of generalised coordinates
t, T	Transformation matrices
z	Column matrix of deflections
Z	Matrix of deflection coefficients
y, ω^2	Coordinates of Graphical Representation—*see* Section 4.3
α, β, γ	Typical finite elements of matrix t
ν	Frequency parameter
υ	Scaled equivalent airspeed
υ_c	Scaled critical flutter equivalent airspeed
σ	Atmospheric relative density

REFERENCE

No.	*Author*	*Title, etc.*
1	Ll. T. Niblett	A graphical representation of the binary flutter equations in normal coordinates. A.R.C. R. & M. 3496 (1966).

APPENDIX A

The Analysis of the Example of Section 4.4

Expressions from Ref. 1 for Significant Features of Figs. 16 and 17

A.1. From Section 4.4, the significant differences between Figs. 16 and 17 are:
(a) limiting y for conic with atmospheric relative density $\sigma = 0$,
(b) effect of atmospheric relative density σ on limiting y,
(c) slope of conic at higher frequency point at $y = 0$.
From Ref. 1, the limiting y with $\sigma = 0$ is

$$\frac{(e_2 - e_1)}{4g}\{(c_{11} - c_{22}) \pm 2\sqrt{-d}\}$$

where $g = d + \frac{1}{4}(c_{11} - c_{22})^2$, $d = c_{12}c_{21}$ and

$$e_r = \frac{e_{rr}}{e_{11} + e_{22}}.$$

With values of coefficients from Figs. 13 and 14, with $\sigma = 0$,

$$\begin{aligned} & g = c_{12}c_{21} && + \tfrac{1}{4}(c_{11} - c_{22})^2 \\ \text{Set 1} \quad & g = (-2{\cdot}502 \times \underline{0{\cdot}389}) && + 0{\cdot}25(0{\cdot}488 + \underline{1{\cdot}084})^2 \\ & = -0{\cdot}973 && + 0{\cdot}618 = -0{\cdot}355 \\ \text{Set 2} \quad & g = (-2{\cdot}842 \times \underline{0{\cdot}227}) && + 0{\cdot}25(0{\cdot}558 + \underline{0{\cdot}096})^2 \\ & = -0{\cdot}645 && + 0{\cdot}107 = -0{\cdot}538. \end{aligned}$$

It may be seen that the differences in c_{21} and c_{22}, shown underlined above, are largely responsible for the smaller numerical value of g with Set 1 data.
With $\sigma = 0$

$$\text{limiting } y = \frac{(e_2 - e_1)}{4g}\{(c_{11} - c_{22}) \pm 2\sqrt{-c_{12}c_{21}}\}.$$

Set 1,

$$\begin{aligned} y &= \frac{(0{\cdot}883 - 0{\cdot}117)}{4 \times (-0{\cdot}355)}\{(0{\cdot}488 + \underline{1{\cdot}084}) \pm 2\sqrt{2{\cdot}502 \times \underline{0{\cdot}389}}\} \\ &= \frac{0{\cdot}766}{4 \times (-0{\cdot}355)}\{(1{\cdot}572) \pm (1{\cdot}973)\} \\ &= \frac{0{\cdot}766}{4 \times (-0{\cdot}355)} \times (-0{\cdot}401) = 0{\cdot}216. \end{aligned}$$

Set 2,

$$\begin{aligned} y &= \frac{(0{\cdot}883 - 0{\cdot}117)}{4 \times (-0{\cdot}538)}\{(0{\cdot}558 + \underline{0{\cdot}096}) \pm 2\sqrt{2{\cdot}842 \times \underline{0{\cdot}227}}\} \\ &= \frac{0{\cdot}766}{4 \times (-0{\cdot}538)}\{(0{\cdot}654) \pm 1{\cdot}606\} \\ &= \frac{0{\cdot}766}{4 \times (-0{\cdot}538)} \times (-0{\cdot}952) = 0{\cdot}339. \end{aligned}$$

It may be seen that c_{21} and c_{22}, shown underlined above, are responsible for differences in numerator and denominator (*via* the value of g) and on the limiting values of y.
With finite σ,

$$\text{limiting } y = \frac{(e_2 - e_1)}{4g}\left\{(c_{11} - c_{22}) - \frac{b}{(e_2 - e_1)} \pm 2\sqrt{-\frac{b(c_{11}e_2 - c_{22}e_1)}{(e_2 - e_1)} + \frac{b^2 e_1 e_2}{(e_2 - e_1)^2} - c_{12}c_{21}}\right\}$$

where $b = \sigma[b_{11}b_{22} - b_{12}b_{21}]$.

	Set 1	Set 2
$\frac{(e_2 - e_1)}{4g}$	$\frac{0{\cdot}766}{4 \times (-0{\cdot}425)} = -0{\cdot}451$	$\frac{0{\cdot}766}{4 \times (-0{\cdot}407)} = -0{\cdot}471$
$(c_{11} - c_{22})$	$0{\cdot}488 + \underline{1{\cdot}084} = \underline{1{\cdot}572}$	$0{\cdot}588 + \underline{0{\cdot}096} = \underline{0{\cdot}654}$
$-\frac{b}{(e_2 - e_1)}$	$-\frac{0{\cdot}322\sigma}{0{\cdot}766} = -0{\cdot}420\sigma$	$-\frac{0{\cdot}396\sigma}{0{\cdot}766} = -0{\cdot}517\sigma$
$-\frac{b(c_{11}e_2 - c_{22}e_1)}{(e_2 - e_1)}$	$-\frac{0{\cdot}322\sigma}{0{\cdot}766}(0{\cdot}488 \times 0{\cdot}883 + \underline{1{\cdot}084} \times 0{\cdot}117)$	$-\frac{0{\cdot}396\sigma}{0{\cdot}766}(0{\cdot}558 \times 0{\cdot}883 + \underline{0{\cdot}096}) \times 0{\cdot}117)$
	$= -0{\cdot}420(0{\cdot}431 + 0{\cdot}127)$	$= -0{\cdot}517(0{\cdot}493 + 0{\cdot}011)$
	$= -0{\cdot}234\sigma$	$= 0{\cdot}261\sigma$
$\frac{b^2e_1e_2}{(e_2 - e_1)^2}$	$\frac{0{\cdot}322^2\sigma^2 \times 0{\cdot}117 \times 0{\cdot}883}{(0{\cdot}766^2)}$	$\frac{0{\cdot}396^2\sigma^2 \times 0{\cdot}117 \times 0{\cdot}883}{(0{\cdot}766^2)}$
	$= 0{\cdot}018\sigma^2$	$= 0{\cdot}028\sigma^2$
$-c_{12}c_{21}$	$2{\cdot}502 \times 0{\cdot}389 = \underline{0{\cdot}973}$	$2{\cdot}842 \times 0{\cdot}227 = \underline{0{\cdot}645}$

Therefore, with $\sigma = 1$.

Set 1, limiting $y = -0{\cdot}451\{\underline{1{\cdot}572} - 0{\cdot}420 \pm 2\sqrt{-0{\cdot}234 + 0{\cdot}018 + \underline{0{\cdot}973}}\}$

$= -0{\cdot}451\{1{\cdot}152 \pm 1{\cdot}742\}$

$= (-0{\cdot}451) \times (0{\cdot}590) = 0{\cdot}266.$

Set 2, limiting $y = -0{\cdot}471\{\underline{0{\cdot}654} - 0{\cdot}517 \pm 2\sqrt{-0{\cdot}261 + 0{\cdot}028 + \underline{0{\cdot}645}}\}$

$= -0{\cdot}471\{0{\cdot}137 \pm 1{\cdot}284\}$

$= (-0{\cdot}471) \times (-1{\cdot}147) = 0{\cdot}540.$

It may be seen that differences in c_{21} and c_{22} (these coefficients or terms significantly affected by them are underlined above) are largely responsible for the differences in limiting y, with $\sigma = 1$.

APPENDIX B

B.1. Definitions of Quasi-Steady Aerodynamic Derivatives

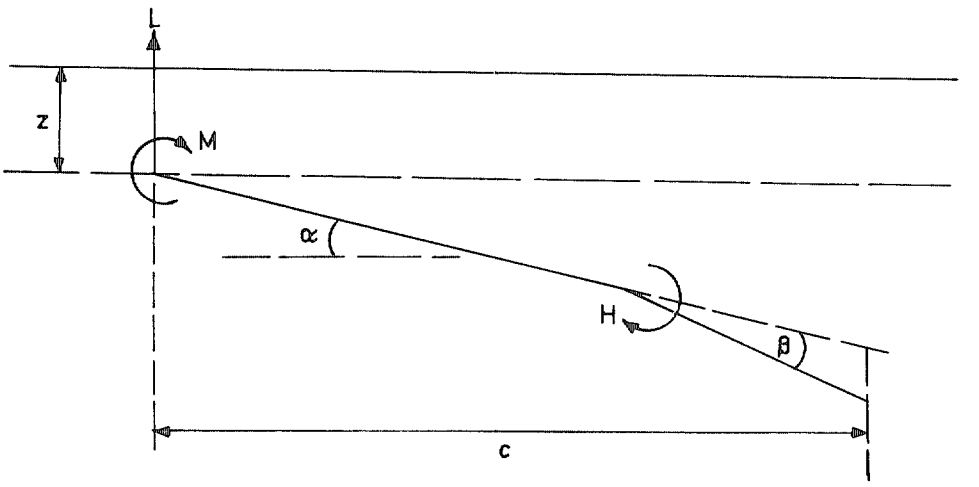

per unit span

$$L = \rho V^2 c[L_\alpha \alpha + L_\beta \beta],$$
$$M = \rho V^2 c^2[M_\alpha \alpha + M_\beta \beta]$$

and

$$H = \rho V^2 c^2[H_\alpha \alpha + H_\beta \beta]$$

where $L = l_x + ivl_\alpha - v^2 l_{\ddot{x}}$ etc., and β may refer to upper or lower rudders.

B.2. Position of Local Aerodynamic Centre

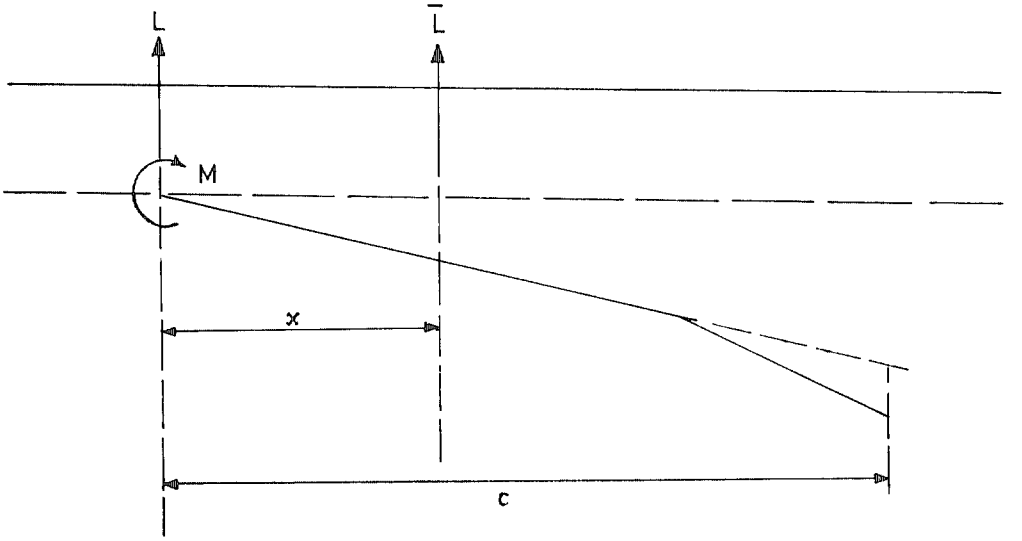

Lift $\bar{L}$ acts at x aft of leading edge, with

$$\bar{L} = L \quad \text{and} \quad Lx + M = 0$$

therefore

$$x = -\frac{M}{L},$$

therefore due to α,

$$x = \frac{-\rho V^2 c^2 m_\alpha \alpha}{\rho V^2 c l_\alpha \alpha} = -\frac{c m_\alpha}{l_\alpha},$$

i.e. due to α, L acts at

$$\left(\frac{x}{c}\right) = \frac{(-m_\alpha)}{l_\alpha} \qquad \text{aft of leading edge}$$

due to β,

$$x = \frac{-\rho V^2 c^2 m_\beta \beta}{\rho V^2 c l_\beta \beta} = \frac{c m_\beta}{l_\beta},$$

i.e. due to β, L act at

$$\left(\frac{x}{c}\right) = \frac{(-m_\beta)}{l_\beta} \qquad \text{aft of leading edge.}$$

TABLE 1

Arbitrary Mode Scaled Frequencies in Example

Mode	Fin and fuselage ($K = \infty$)		Rudders	
		$K^{\frac{1}{2}} = 0{\cdot}324$	$K^{\frac{1}{2}} = 0{\cdot}725$	$K^{\frac{1}{2}} = 1{\cdot}0$
1	0·62	—	—	—
2	1·47	—	—	—
3	1·78	—	—	—
4	2·23	—	—	—
5	2·56	—	—	—
Upper rudder	—	0·93	2·08	2·87
Lower rudder	—	0·67	1·49	2·05

TABLE 2

Normal Mode Scaled Frequencies in Example

Mode \ $K^{\frac{1}{2}}$	0·324	0·725	1·0
1	0·55	0·61	0·62
2	0·67	1·12	1·27
3	1·08	1·61	1·70
4	1·79	1·89	1·97
5	2·39	2·50	2·52
6	2·74	3·72	4·78
7	7·53	9·07	10·59

TABLE 3

Scaled Flutter Speeds and Frequencies in Example

Set 1 Aerodynamics

$K^{\frac{1}{2}}$	7 modes		Point	Modes remaining after degree-of-freedom dropping			Binary	
	v_c	f_c		Modes	v_c	f_c	v_c	f_c
0·324	0·53	1·01	a.	1–2–3	0·52	1·01	0·53	1·02
	1·46	1·84	d.	2–3–4	1·56	1·83	1·55	1·82
0·725	1·17	1·25	b.	1–3	1·17	1·35	1·17	1·35
	1·97	2·00	e.	1–2–3–4–5	1·86	1·97	1·87	1·95
	2·40	2·08	e.	*	*	*	2·58	2·14
1·0	1·30	1·24	c.	1–3	1·35	1·34	1·35	1·34

* This point is an upper critical flutter speed to which the degree-of-freedom dropping procedure does not apply, but which is represented by the binary for the corresponding lower critical flutter speed.

TABLE 4

Scaled Flutter Speeds and Frequencies in Example

Set 2 Aerodynamics

$K^{\frac{1}{2}}$	7 modes		Point	Modes remaining after degree-of-freedom dropping			Binary	
	v_c	f_c		Modes	v_c	f_c	v_c	f_c
0·324	0·61	1·02	f.	1–3	0·64	1·03	0·64	1·03
	1·11	1·78	g.	1–2–4	1·18	1·77	1·15	1·77
0·725	1·06	1·86	h.	2–3–4	1·06	1·87	1·06	1·85
	1·83	3·13	j.	3–6	1·96	2·95	1·96	2·95
1·0	1·23	1·94	i.	2–3–4	1·23	1·94	1·27	1·92
	1·80	1·24	k.	1–3	1·88	1·32	1·88	1·32
	2·43	4·14	l.	3–6	2·52	3·93	2·52	3·93

TABLE 5

Values of Aerodynamic Stiffness Derivatives, with Associated Centres of Lift

Derivative	Set 1	Set 2
l_α	1·26	1·31
$(-m_\alpha)$	0·315	0·394
$l_{\beta L}$	0·682	0·686
$(-m_{\beta L})$	0·341	0·501
$(-h_{\beta L})$	0·0181	0·0157
$(-h_{\alpha L})$	0·00137	0·0006
$(-h_{\alpha U})$	−0·0152	0·006
$l_{\beta U}$	0·887	0·881
$(-m_{\beta U})$	0·443	0·590
$(-h_{\beta U})$	0·0252	0·0296
$(-m_\alpha)/l^*_\alpha$	0·25	0·30
$(-m_{\beta L})/l^*_{\beta L}$	0·50	0·73
$(-m_{\beta U})/l^*_{\beta U}$	0·50	0·67

* *See* Appendix B.2—values are centres of lift in fractions of chord aft of leading edge.

TABLE 6

Point c., Fig. 2—Contribution to Aerodynamic Coefficients

Coefficients c_{21} and c_{22} from the Derivatives

For c_{21}

Due to derivative	Set 1	Set 2
l_α	0·519	0·538
$(-m_\alpha)$	−0·206*	−0·258*
$l_{\beta L}$	0·069	0·069
$(-m_{\beta L})$	−0·024	−0·035
$(-h_{\beta L})$	−0·010	−0·009
$(-h_{\alpha L})$	0·000	0·000
$(-h_{\alpha U})$	0·022	−0·009
$l_{\beta U}$	0·280	0·276
$(-m_{\beta U})$	−0·229*	−0·304*
$(-h_{\beta U})$	−0·032	−0·041
	$\therefore c_{21} = 0{\cdot}389$	$\therefore c_{21} = 0{\cdot}227$

For c_{22}

l_α	−1·499	−1·554
$(-m_\alpha)$	0·649*	0·812*
$l_{\beta L}$	−0·116	−0·116
$(-m_{\beta L})$	0·036	0·053
$(-h_{\beta L})$	0·017	0·015
$(-h_{\alpha L})$	0·000	0·000
$(-h_{\alpha U})$	−0·069	0·027
$l_{\beta U}$	−2·395	−2·361
$(-m_{\beta U})$	2·013*	2·681*
$(-h_{\beta U})$	0·280	0·347
	$\therefore c_{22} = -1{\cdot}084$	$\therefore c_{22} = -0{\cdot}096$

* Significant differences.

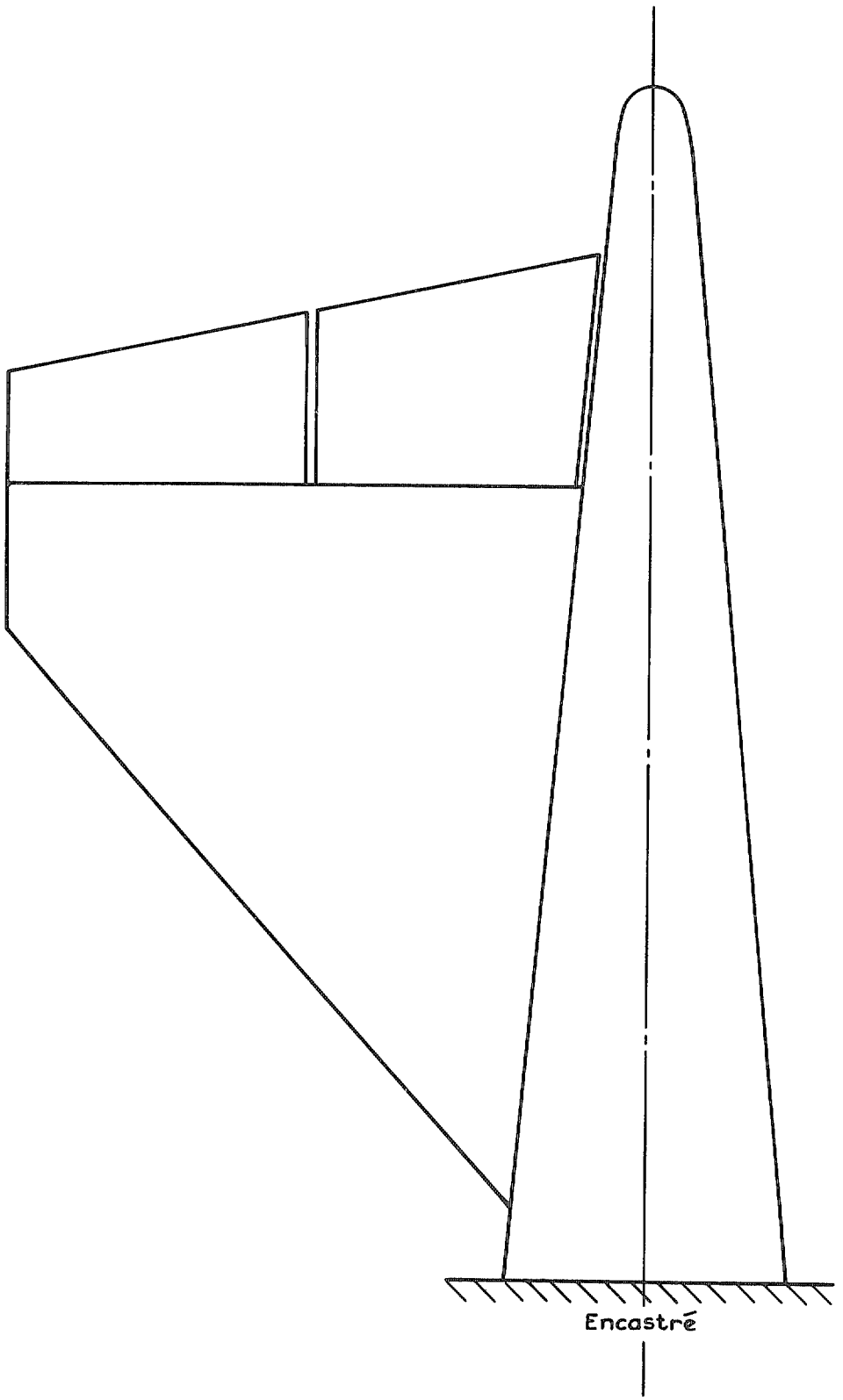

FIG. 1. Geometry of example.

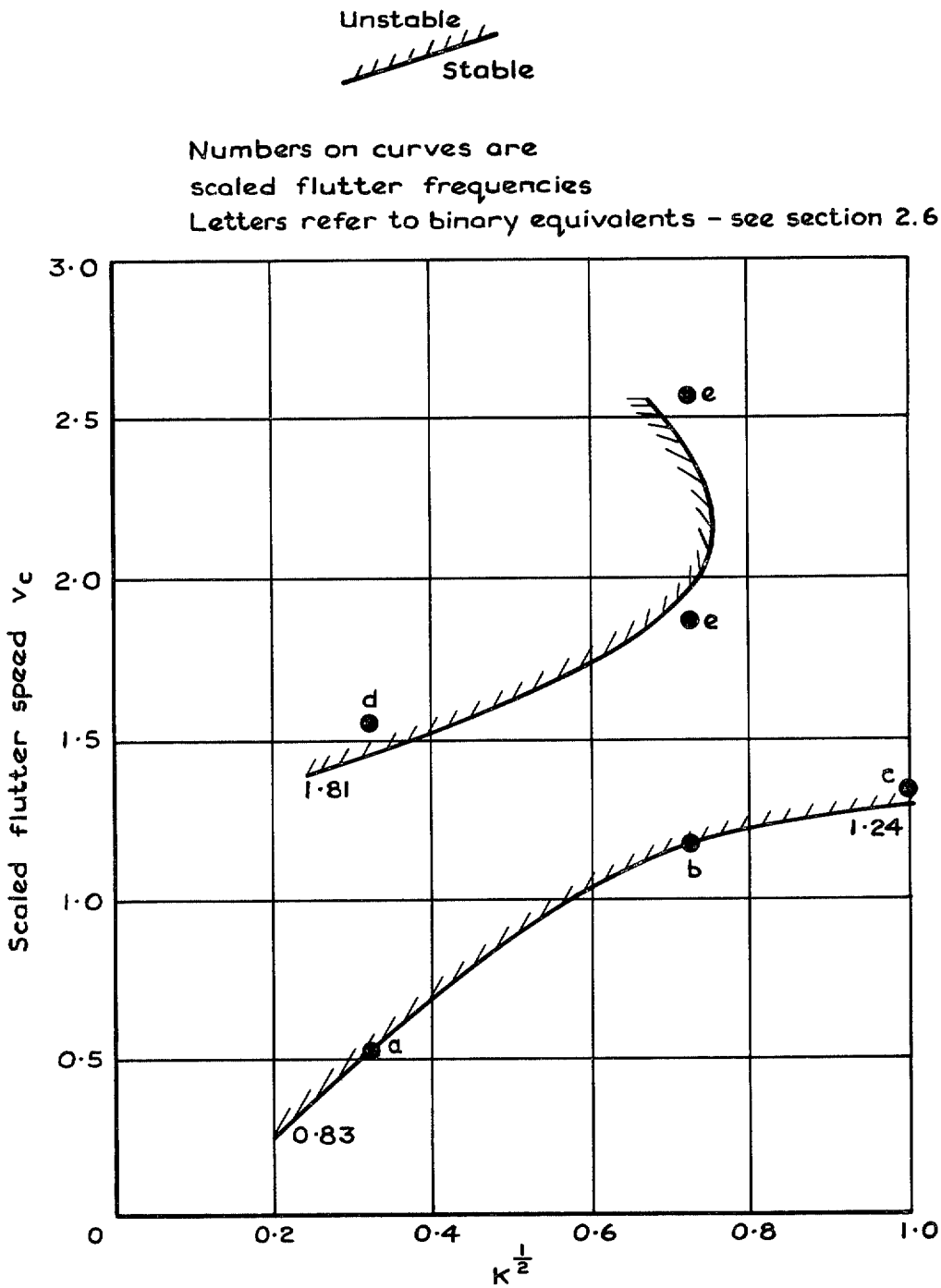

FIG. 2. Variation of scaled flutter speed v_c with scaled jack stiffness K—Set 1 aerodynamics.

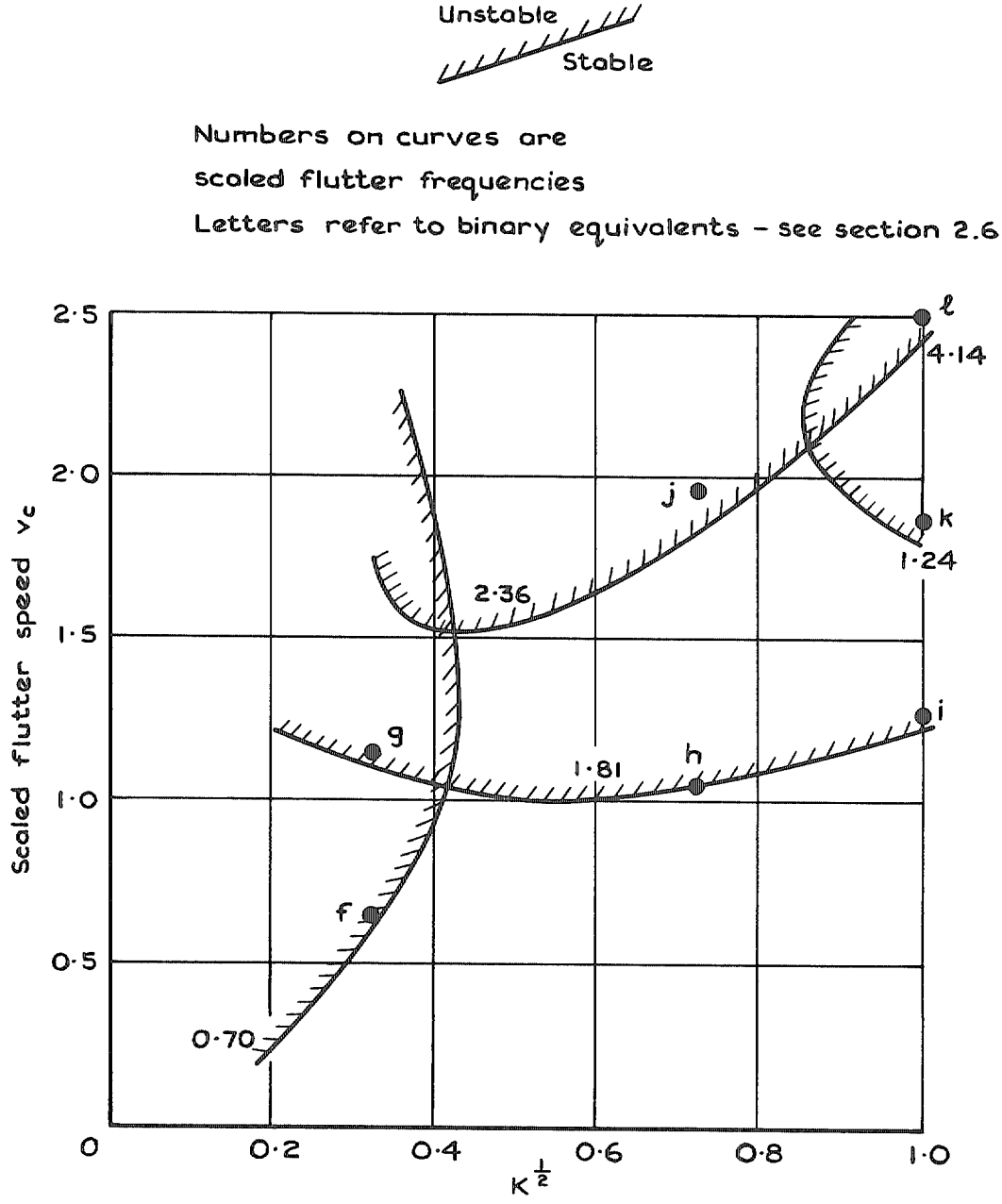

FIG. 3. Variation of scaled flutter speed v_c with scaled jack stiffness K—Set 2 aerodynamics.

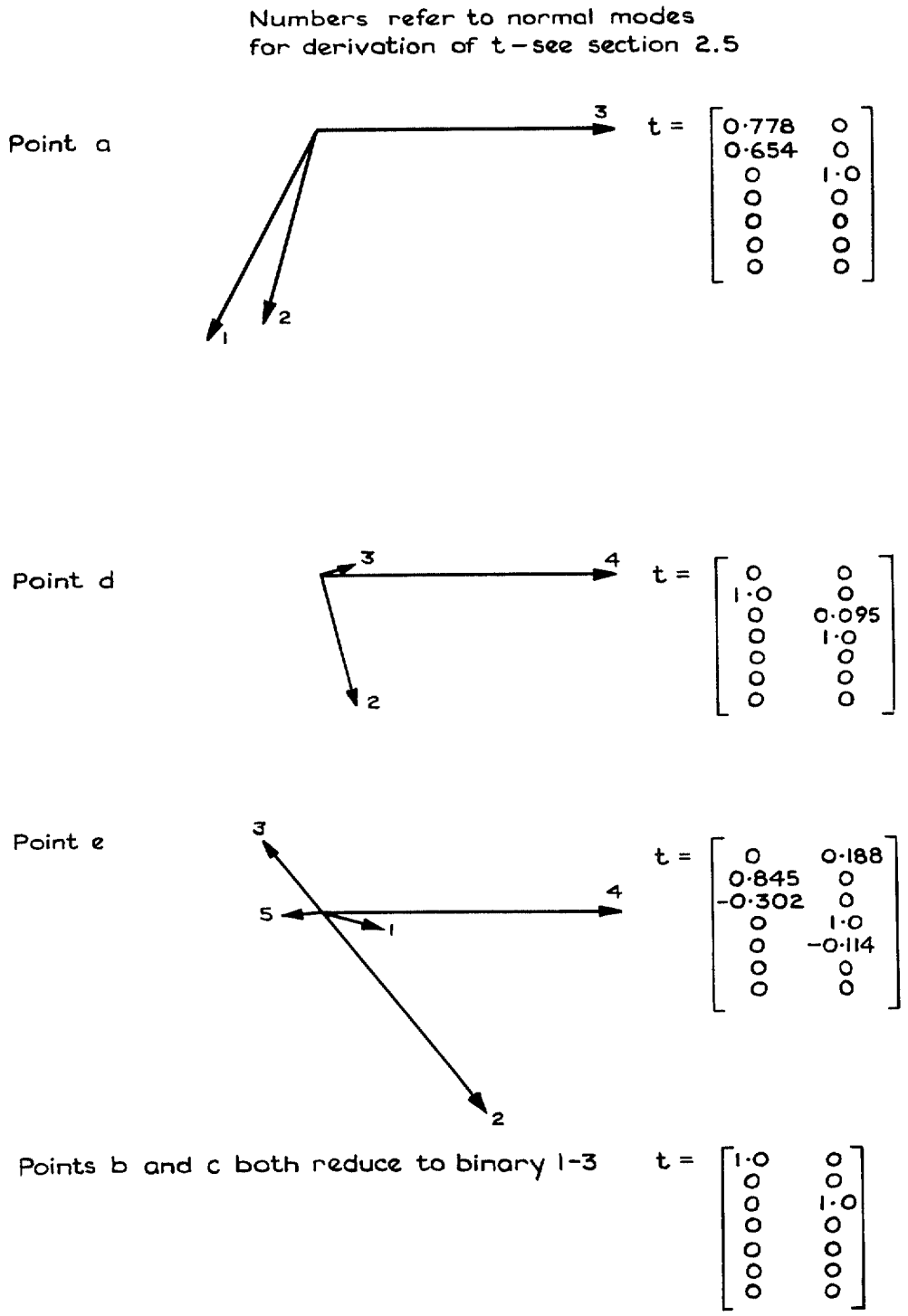

FIG. 4. Critical flutter vectors for reduced systems output by Stage 2—Set 1 aerodynamics.

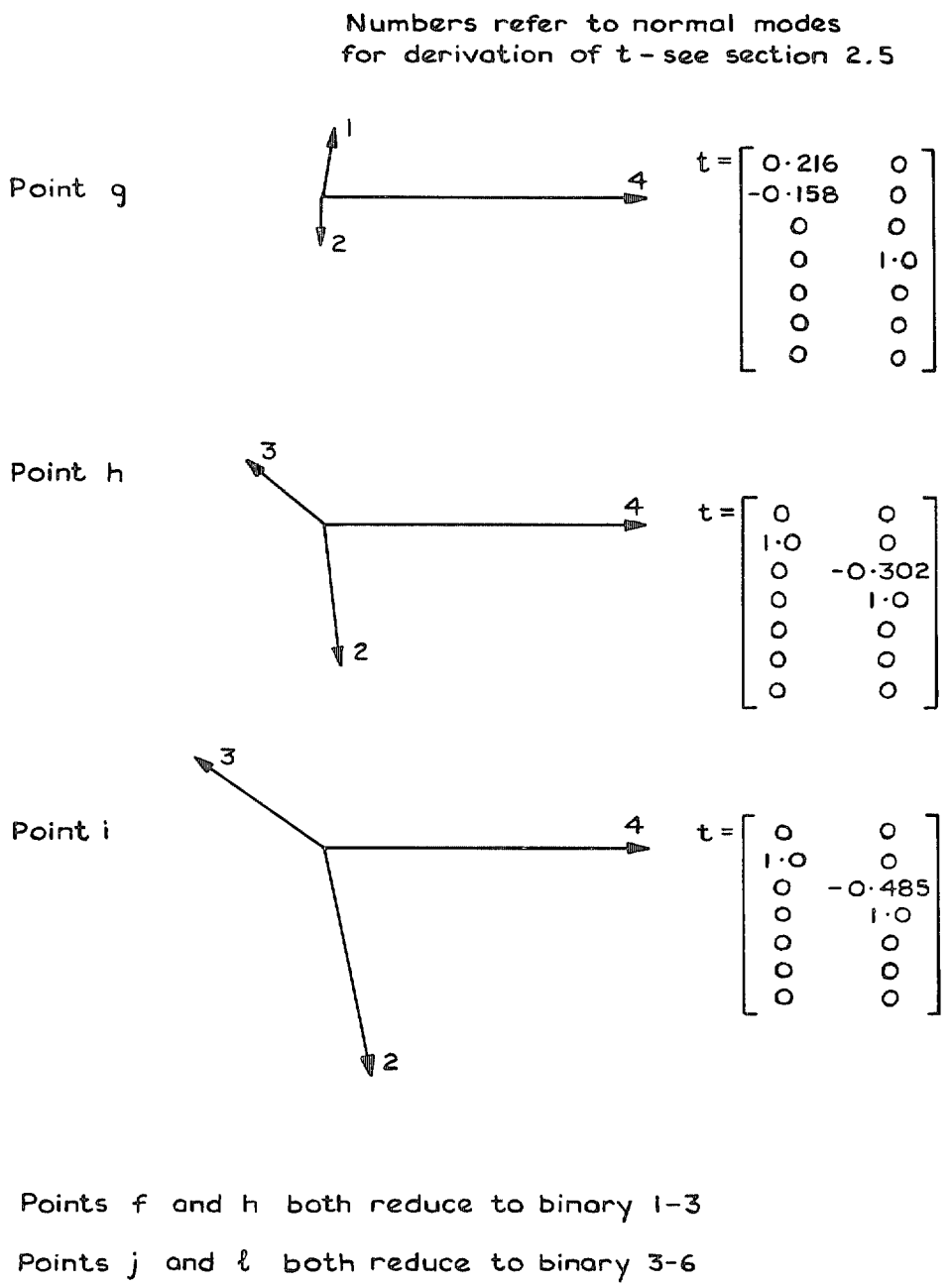

FIG. 5. Critical flutter vectors for reduced systems output by Stage 2—Set 2 aerodynamics.

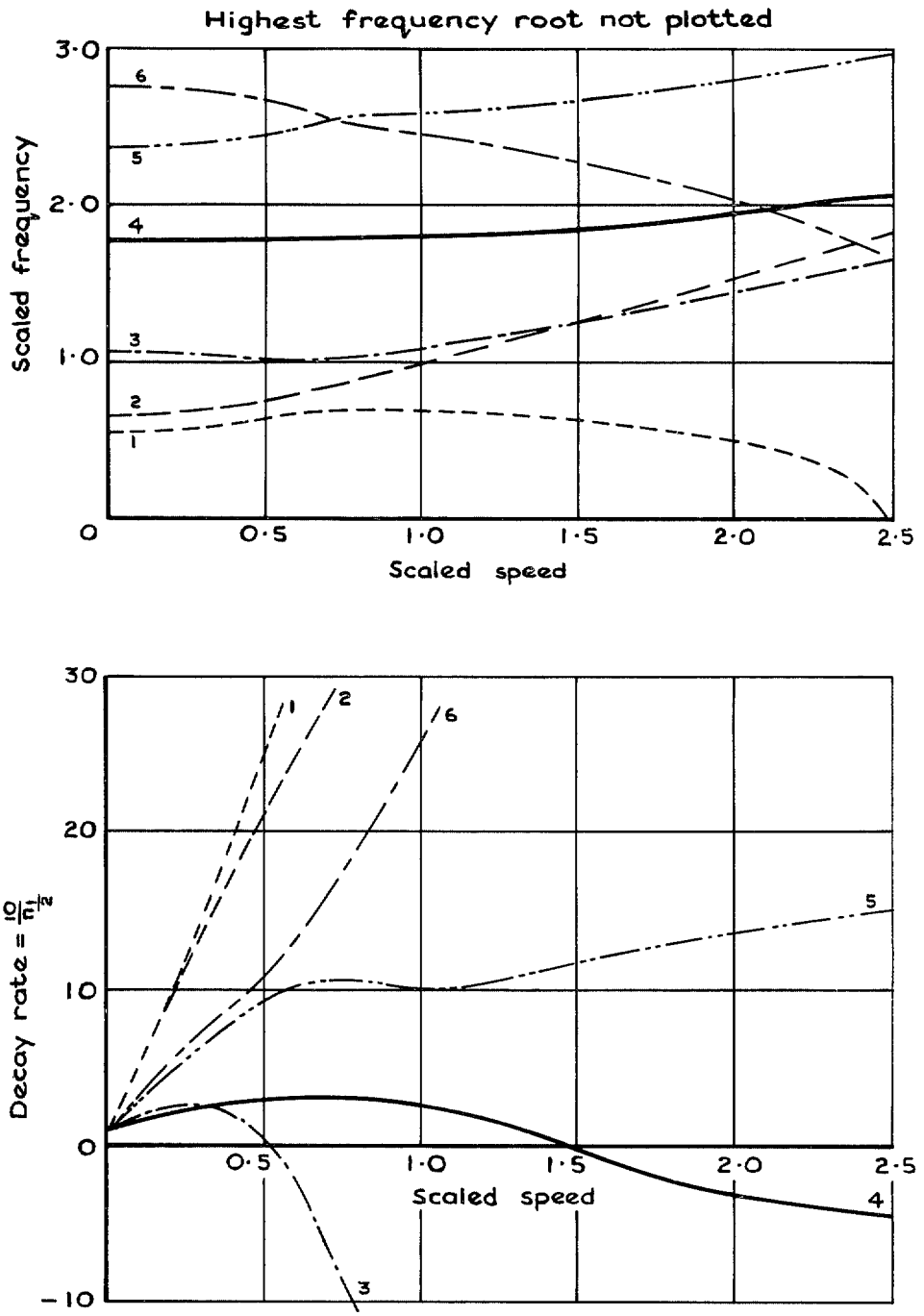

FIG. 6. Variation of roots with speed, 7 degrees-of-freedom—Set 1 aerodynamics, $K^{\frac{1}{2}} = 0{\cdot}324$.

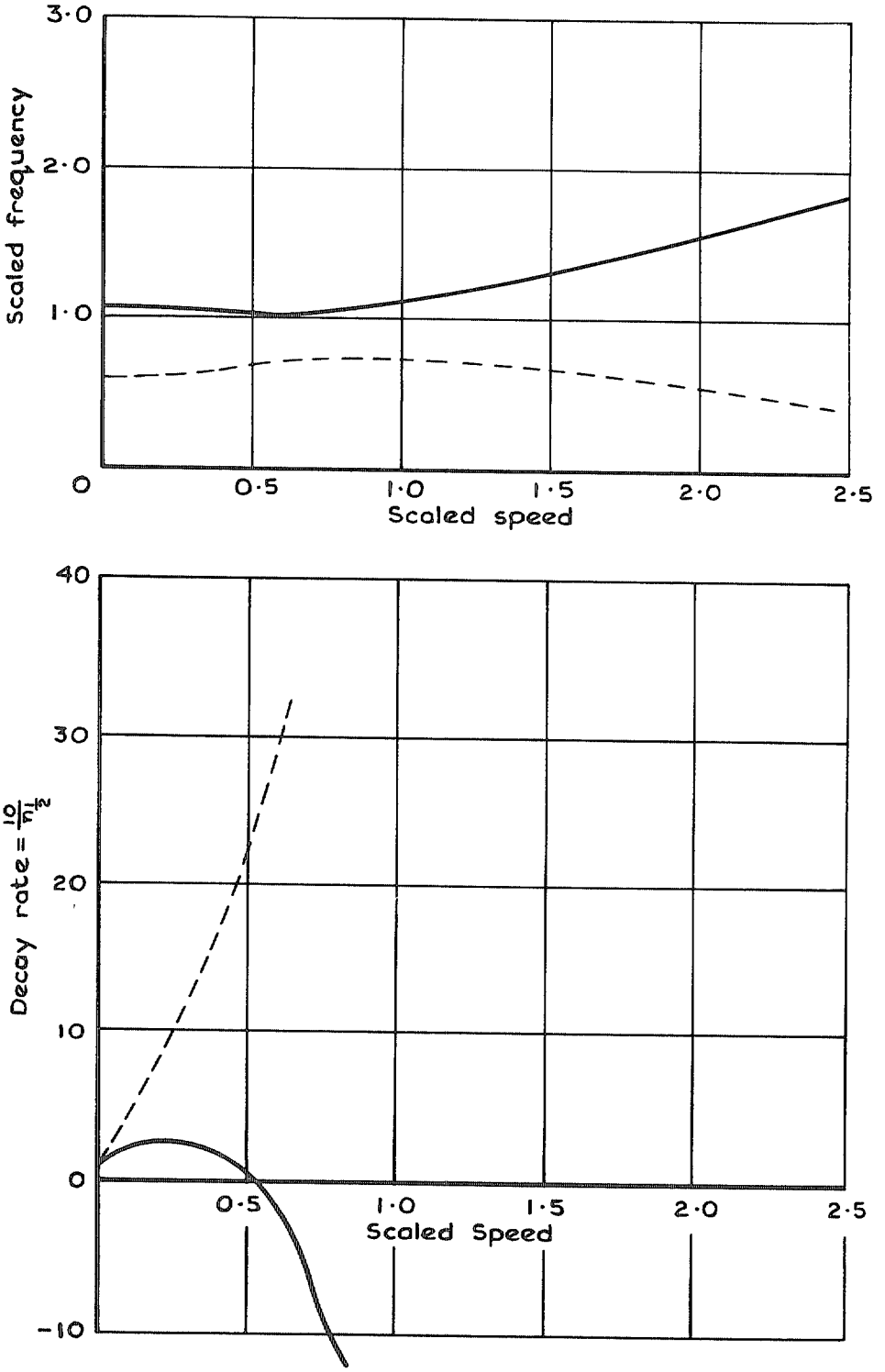

FIG. 7. Variation of roots with speeds, point a binary—Set 1 aerodynamics, $K^{\frac{1}{2}} = 0{\cdot}324$.

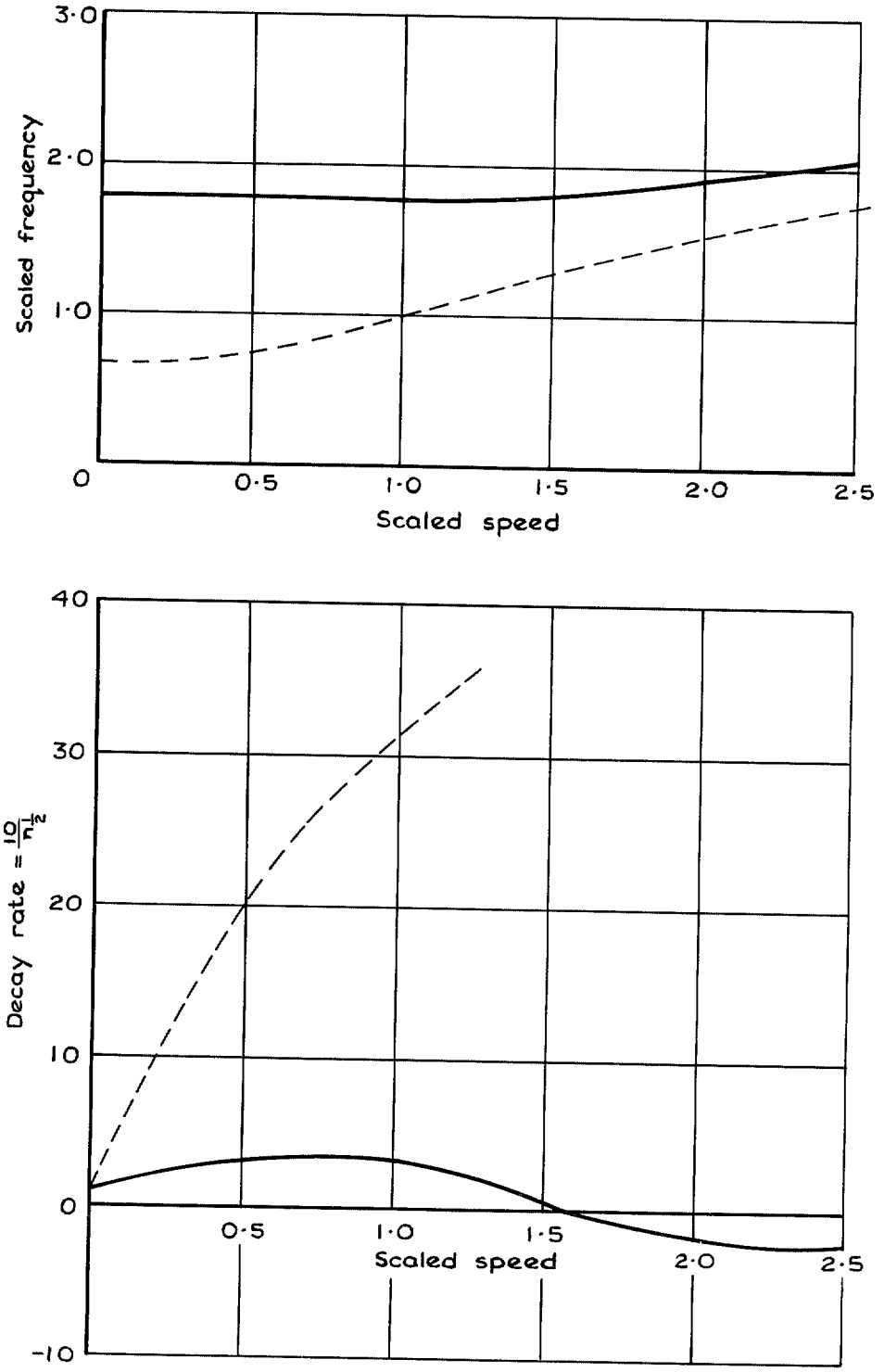

FIG. 8. Variation of roots with speed, point d binary—Set 1 aerodynamics, $K^{\frac{1}{2}} = 0{\cdot}324$.

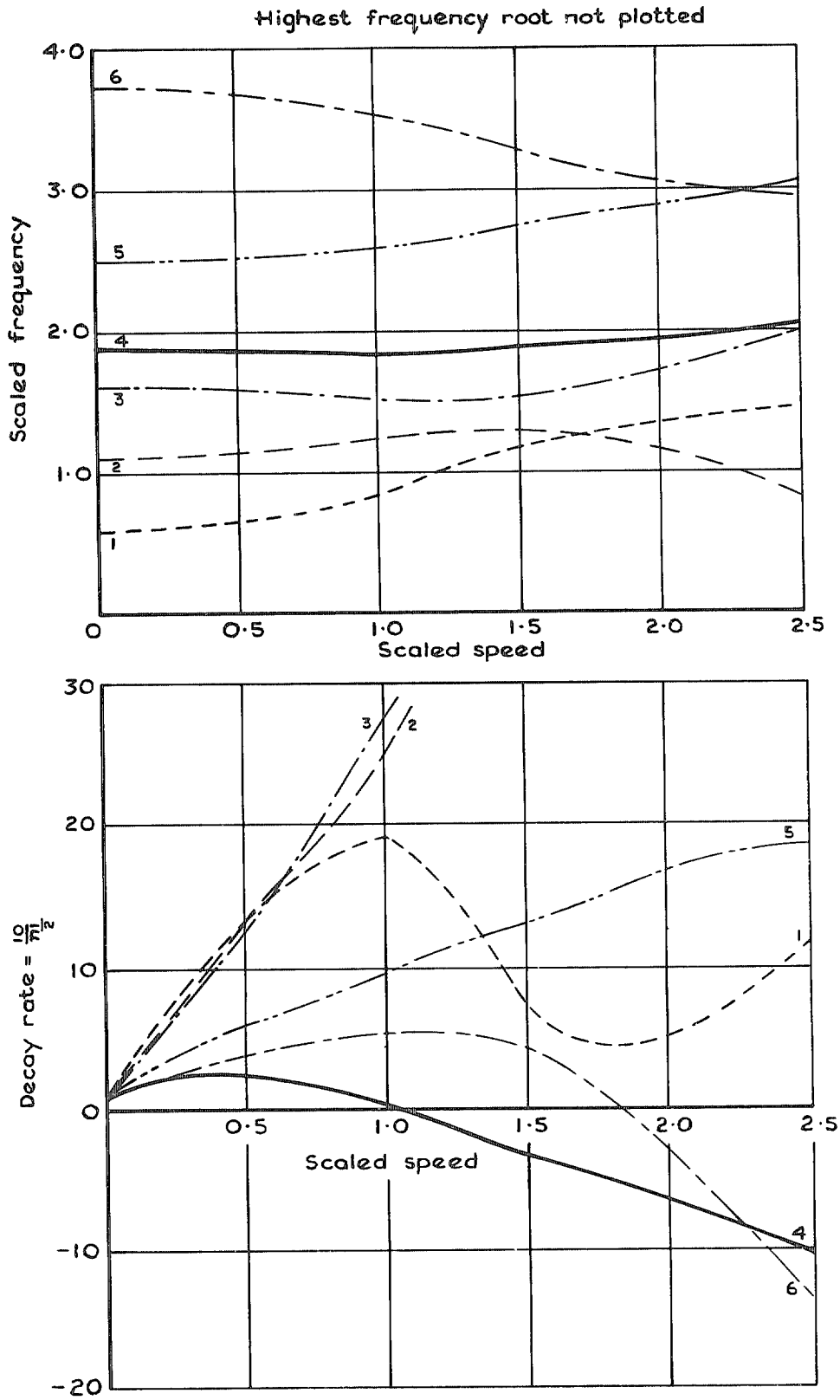

FIG. 9. Variation of roots with speed, 7 degrees-of-freedom— Set 2 aerodynamics, $K^{\frac{1}{2}} = 0{\cdot}725$.

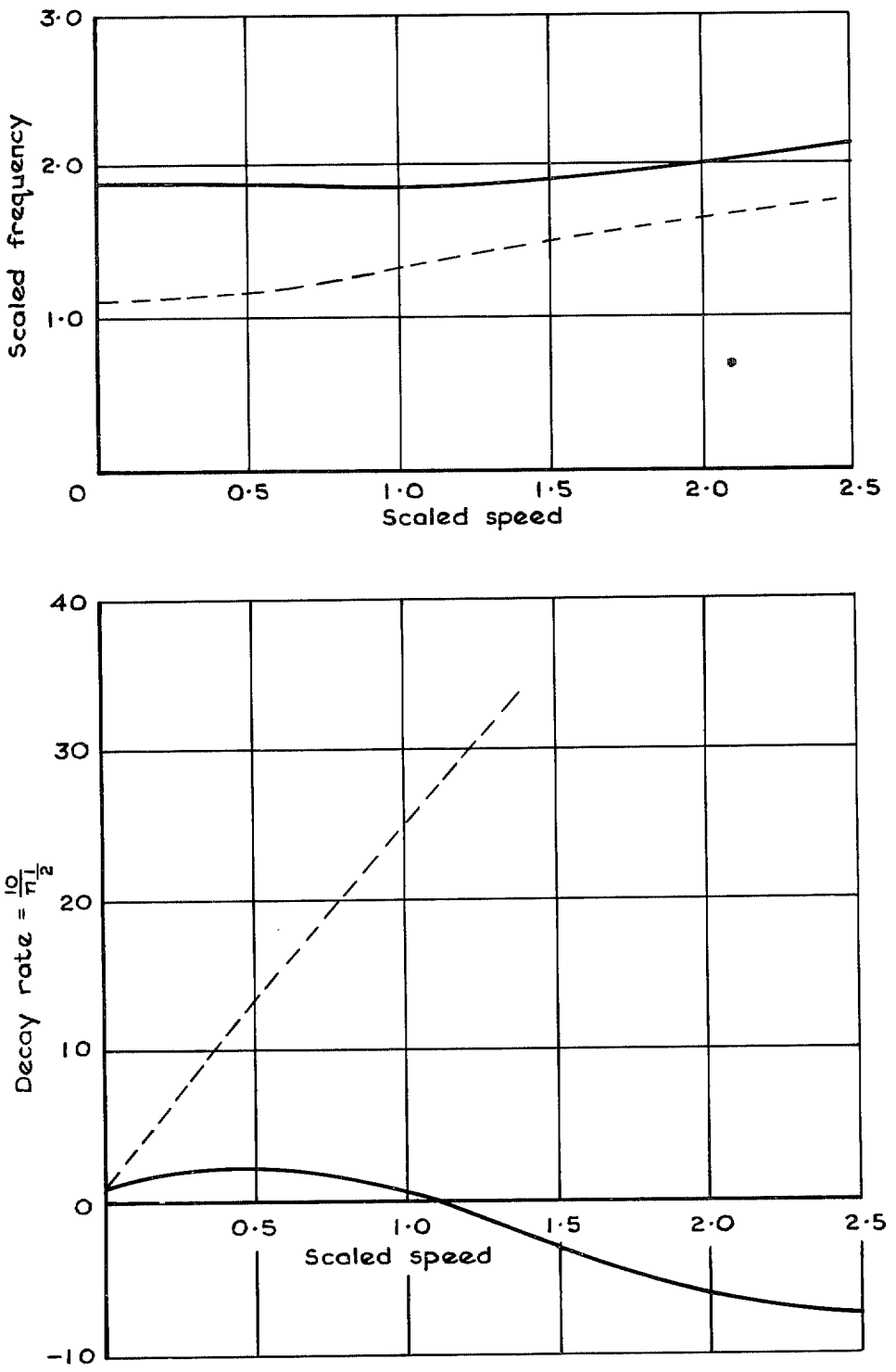

FIG. 10. Variation of roots with speed, point h binary—Set 2 aerodynamics, $K^{\frac{1}{2}} = 0{\cdot}725$.

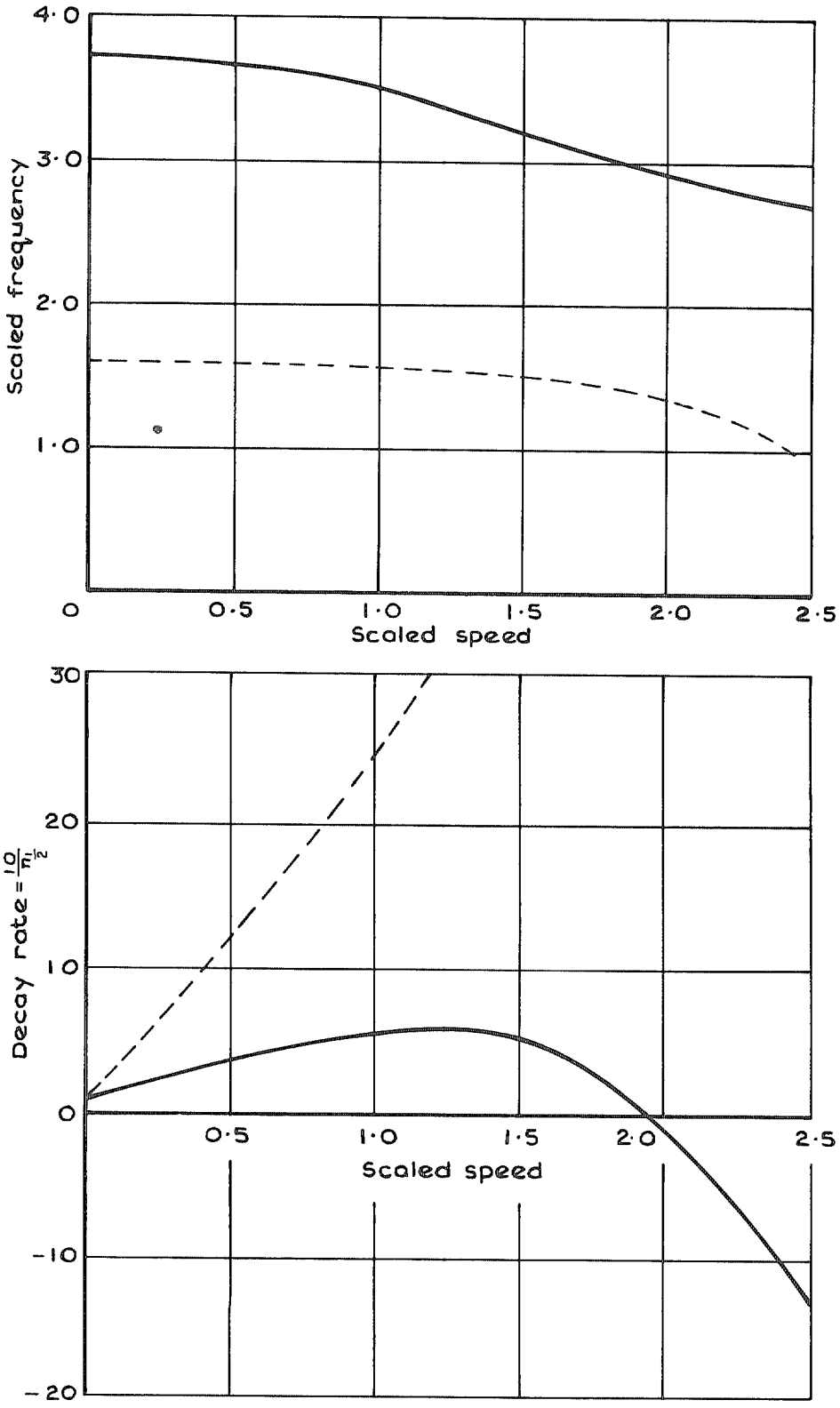

FIG. 11. Variation of roots with speed, point j binary—Set 2 aerodynamics, $K^{\frac{1}{2}} = 0{\cdot}725$.

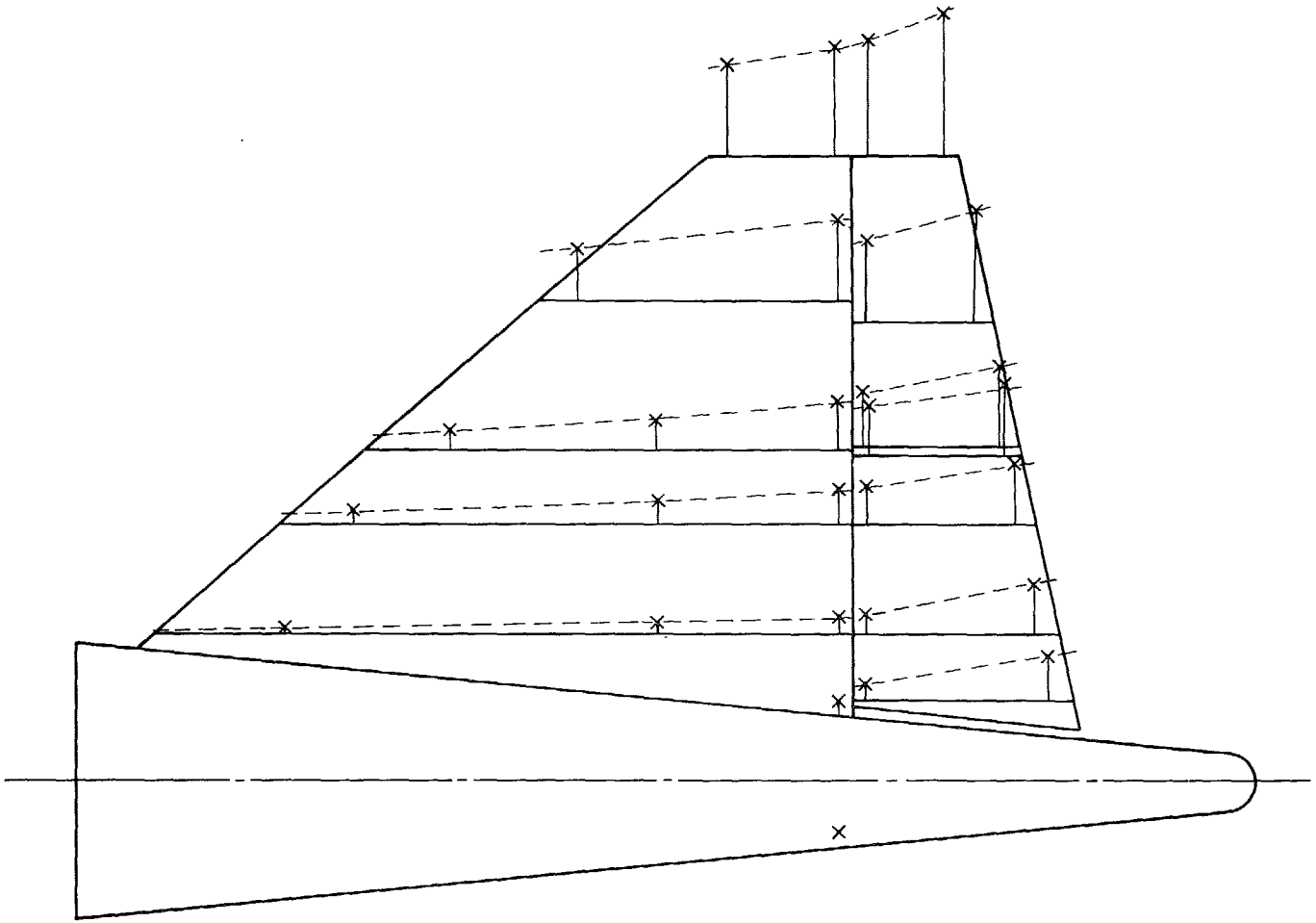

FIG. 1.. Binary point *c*—1st mode, scaled frequency = 0·62.

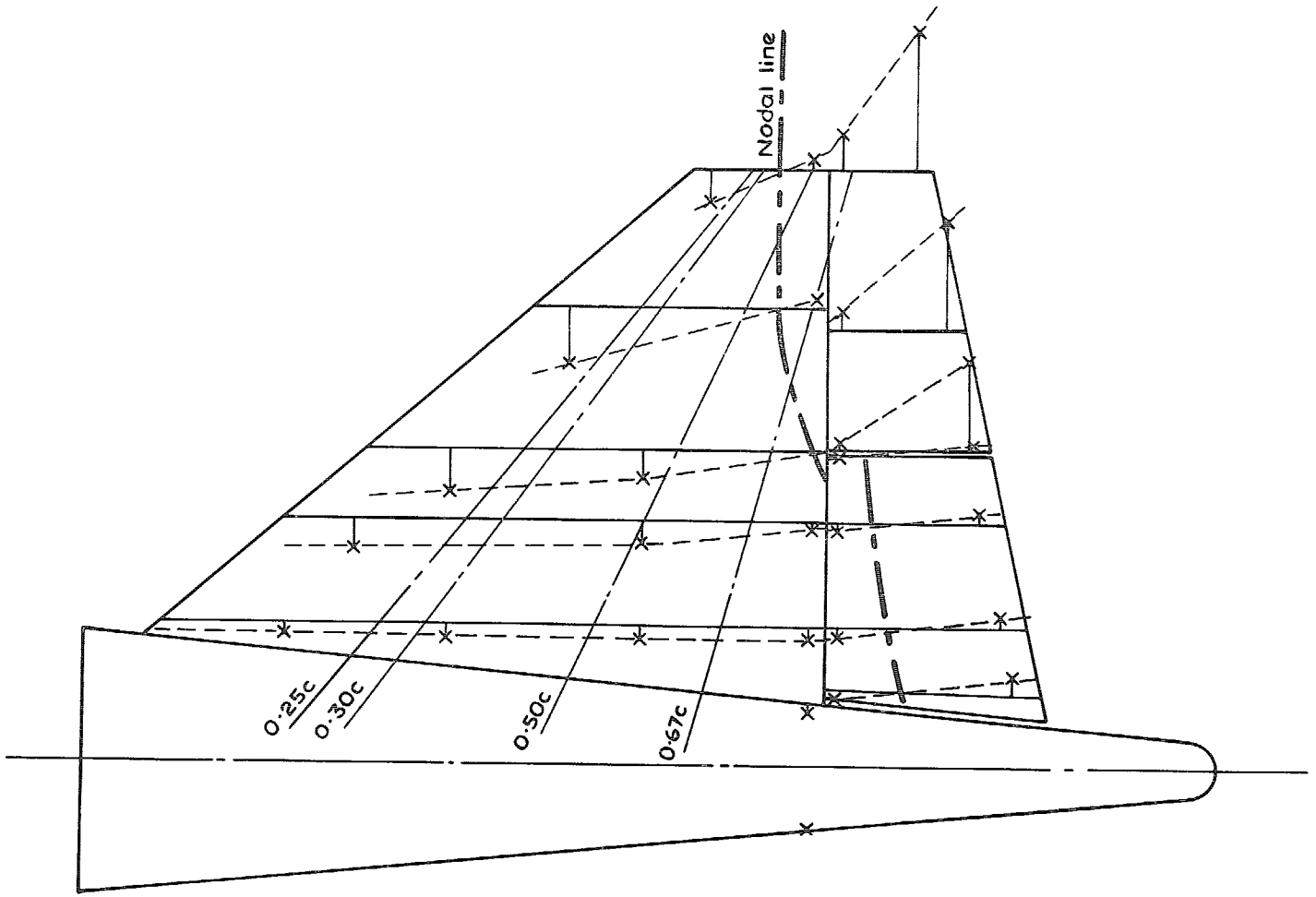

FIG. 13. Binary point c—2nd mode, scaled frequency = 1·70.

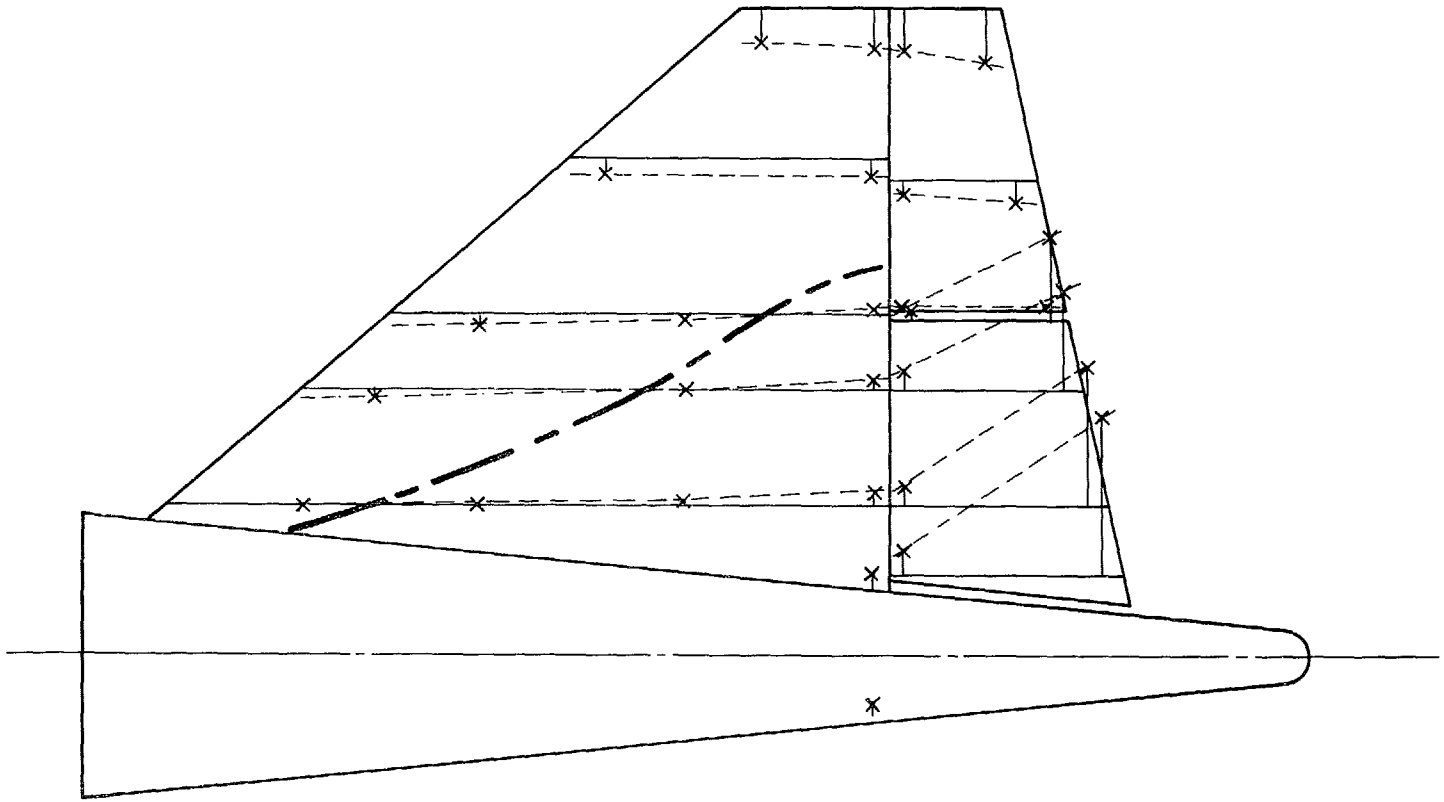

FIG. 14. Binary point *i*—1st mode, scaled frequency = 1·27.

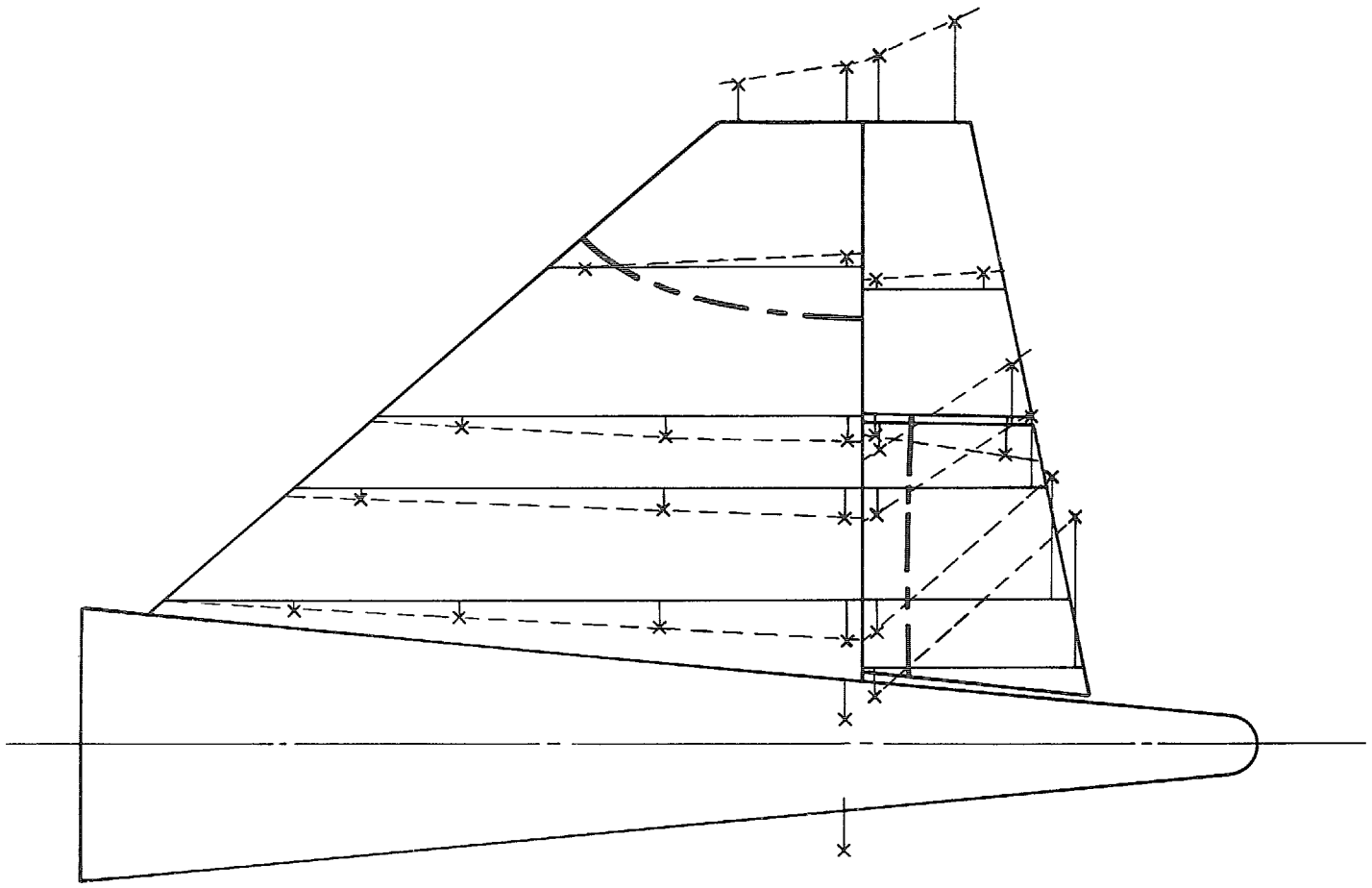

FIG. 15. Binary point *i*—2nd mode, scaled frequency = 1·92.

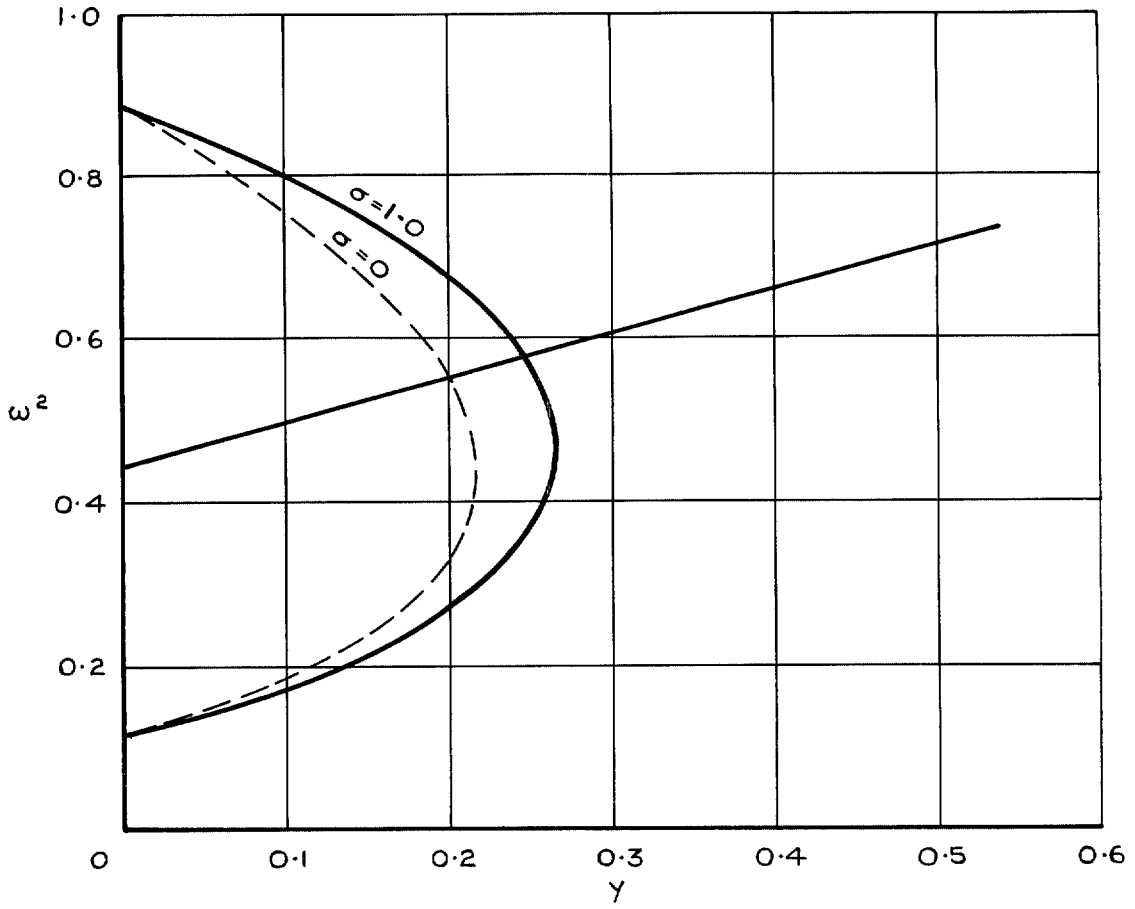

$$\bar{\bar{A}} = \begin{bmatrix} 1\cdot0 & 0 \\ 0 & 1\cdot0 \end{bmatrix}$$

$$\bar{\bar{B}} = \begin{bmatrix} 0\cdot373 & -0\cdot653 \\ 0\cdot171 & 0\cdot563 \end{bmatrix}$$

$$\bar{\bar{C}} = \begin{bmatrix} 0\cdot488 & -2\cdot502 \\ 0\cdot389 & -1\cdot084 \end{bmatrix}$$

$$\bar{\bar{E}} = \begin{bmatrix} 0\cdot382 & 0 \\ 0 & 2\cdot885 \end{bmatrix}$$

FIG. 16.—Graphical representation of binary point *c*—Set 1 aerodynamics.

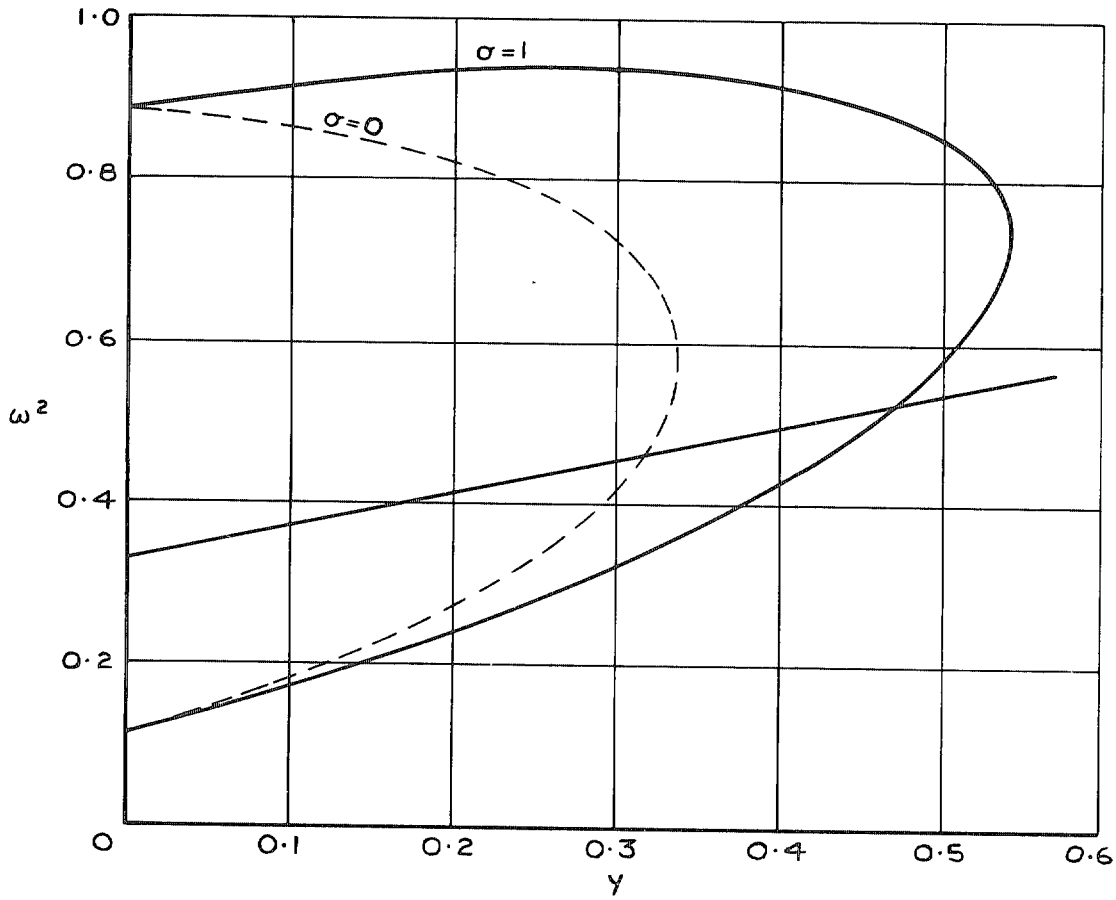

$$\bar{\bar{A}} = \begin{bmatrix} 1{\cdot}0 & 0 \\ 0 & 1{\cdot}0 \end{bmatrix}$$

$$\bar{\bar{B}} = \begin{bmatrix} 0{\cdot}394 & -0{\cdot}655 \\ -0{\cdot}033 & 1{\cdot}059 \end{bmatrix}$$

$$\bar{\bar{C}} = \begin{bmatrix} 0{\cdot}558 & -2{\cdot}842 \\ 0{\cdot}227 & -0{\cdot}096 \end{bmatrix}$$

$$\bar{\bar{E}} = \begin{bmatrix} 0{\cdot}382 & 0 \\ 0 & 2{\cdot}885 \end{bmatrix}$$

FIG. 17. Graphical representation of binary point c but with Set 2 aerodynamics.

Printed in England for Her Majesty's Stationery Office by J. W. Arrowsmith Ltd., Bristol BS3 2NT.
Dd. 505374 K5 1/75.

HER MAJESTY'S STATIONERY OFFICE

Government Bookshops

49 High Holborn, London WC1V 6HB
13a Castle Street, Edinburgh EH2 3AR
41 The Hayes, Cardiff CF1 1JW
Brazennose Street, Manchester M60 8AS
Southey House, Wine Street, Bristol BS1 2BQ
258 Broad Street, Birmingham B1 2HE
80 Chichester Street, Belfast BT1 4JY

Government publications are also available through booksellers

ISBN 0 11 470910 6